INSTITUTE OF PLASMA PHYSICS

NAGOYA UNIVERSITY

RESEARCH REPORT

NAGOYA, JAPAN

The Record of Symposium on Plasma Diagnostics

IPPJ-181 December 1973

February 21, 1973

Institute of Plasma Physics
Nagoya University
Nagoya

Further communication about this report is to be sent to the Research Information Center, Institute of Plasma Physics, Nagoya University, Nagoya, JAPAN.

Table of Contents

1) Design of Sin-Cos-Probe for ETL-TPE-1: *Eiichi Yahagi* 1

2) Low Frequency Oscillation in a High Density Plasma: *Yasushi Nishida and Kazushige Ishii* 9

3) Distribution Measurement in k-space of Ion Acoustic Wave by Microwave Scattering: *Atsushi Mase, Takumi Yamamoto and Takashige Tsukishima* 13

4) Review of Particle Diagnostics: *N. Inoue* 23

5) Calibration of Electron Bombardment Detector for Fast Neutral Particles (Abstract only): *Hajime Ishimaru and Kohtaro Satoh* 30

6) Spectral Line Profile and Its Application: *Toshiatsu Oda* 31

7) An Attempt to Determine Electron Temperature by the Measurement of Lyman Step of Helium Ion Continuum: *S. Ohsumi and T. Ishimura* 42

8) Measurement of the Absolute Intensity of Radiation in the Soft X-Ray and Extreme Ultraviolet Region: *H. Sugawara, T. Sasaki and T. Oda* 48

9) Laser Light Scattering from a Turbulently Heated Plasma: *K. Kondo* 62

10) Relativistic Corrections to the Spectrum of Scattered Light from a High Temperature Plasma: *Kiyoshi Hayase and Takayoshi Okuda* 70

Design of Sin-Cos-Probe for ETL-TPE-1

Eiichi Yahagi

Electrotechnical Laboratory

1. Magnetic field in a nested toroid

We suppose a toroidal metal shell with the toroidal radius of R_S and the poroidal radius of b including a conducting toroid with the poroidal radius of a in it as shown in Fig.1. The magnetic field between the two surfaces of the inner conductor and the toroidal metal shell must satisfy the boundary condition on the conductor surfaces, where the normal component of the magnetic field equals to zero. The magnetic field, of which lines of force compose Apollonius' circles including the two circular boundary surfaces satisfies the boundary condition. Suppose there is only toroidal component of electric current in the conductors, then the magnetic field has no toroidal component. We consider a Farady tube with infinitishmal cross section, then the magnetic field intensity along the Farady tube is in inverse proportion to the area of the cross section. The area of the cross section is in proportion to $\{\alpha_c-\cos(\theta_c+\phi)\}\times(\alpha_c'-\cos\theta_c)$, and the circumferential line integral along a magnetic line of force is to be the toroidal current included in the contour. That is

$$\int_0^{2\pi} H(C,\theta_c)\,C\,d\theta_c = I_z \qquad (1),$$

where I_z is the toroidal current, C is the radius of the magnetic line of force across the observation point $P(r,\theta)$, θ_c is a clockwise angle from the direction of the deflection of the inner conductor to point P and the origin is the center of the circle made of the magnetic line of force across the point P.

The magnetic field intensity $H(C,\theta_c)$ is written

$$H(C,\theta_c)=g(C)\Psi(C,\theta_c) \tag{2}$$

where

$$\Psi(C,\theta_c)=\frac{1}{\alpha_c-\cos(\theta_c+\phi)}\times\frac{1}{\alpha_c'-\cos\theta_c} \tag{3}$$

$g(C)$ is independent of θ_c and is determined by performing the integral of eq.(1). The integral was solved by means of integration in complex domain. Thus $g(C)$ is expressed as

$$g(C)=\frac{I_z}{2\pi c}\frac{\alpha_c^2+\alpha_c'^2-2\alpha_c\alpha_c'\cos\phi-\sin^2\phi}{\dfrac{\alpha_c'-\alpha_c\cos\phi}{\sqrt{\alpha_c^2-1}}\dfrac{\alpha_c-\alpha_c'\cos\phi}{\sqrt{\alpha_c'^2-1}}} \tag{4}$$

where

$$C=\frac{\sqrt{\left(\alpha_s'-\frac{1+\bar{r}^2}{2\bar{r}}\cos\theta'\right)^2+\left(\frac{1-\bar{r}^2}{2\bar{r}}\right)^2\sin^2\theta'}}{\alpha_s'-\bar{r}\cos\theta'}\,r \tag{5-1},$$

$$\alpha_c=\left\{\alpha_s-\frac{\frac{1-\bar{r}^2}{2}}{\alpha_s'-\bar{r}\cos\theta'}\right\}/\bar{C} \tag{5-2}$$

$$\alpha_c'=\left\{\alpha_s'-\frac{\frac{1-\bar{r}^2}{2}}{\alpha_s'-\bar{r}\cos\theta'}\right\}/\bar{C} \tag{5-3},$$

$$\theta'=\theta-\phi \tag{6}$$

$$\begin{cases}\cos\theta_c=\dfrac{R}{C}\left\{\cos\theta'-\dfrac{\frac{1-\bar{r}^2}{2\bar{r}}}{\alpha_s'-\bar{r}\cos\theta'}\right\} & (7\text{-}1)\\[2ex] \sin\theta_c=\dfrac{r}{C}\sin\theta' & (7\text{-}2)\end{cases}$$

$$\alpha_s=\frac{R_s}{b}\ ,\quad \alpha_s'=\frac{R_s'}{b}=\frac{1-\bar{a}^2+\bar{\Delta}^2}{2\bar{\Delta}}=\frac{1+\bar{\delta}_s^2}{2\bar{\delta}_s} \tag{8},$$

$$\begin{cases}\bar{\delta}=\dfrac{\sigma a^2}{1+\sqrt{1-\sigma_a^2}}\,\bar{a} & (9\text{-}1)\\[2ex] \bar{\delta}_s=\dfrac{\sigma_b^2}{1+\sqrt{1-\sigma_b^2}} & (9\text{-}2)\end{cases}$$

$$\begin{cases} \sigma_a = \dfrac{2\bar{\Delta}\bar{a}}{1-\bar{a}^2-\bar{\Delta}^2} & (10\text{-}1) \\ \sigma_b = \dfrac{2\bar{\Delta}}{1-\bar{a}^2+\bar{\Delta}^2} & (10\text{-}2), \end{cases}$$

in which δ is a distance between the poroidal axis of the inner conductor and the magnetic axis, δ_s is a distance between the poroidal axis of the metal shell and the magnetic axis, Δ is a distance between the poroidal axes of the metal shell and the inner conductor, and - denote normalization by b. If we know α_s', δ_s and Δ will be determined from equations (11) and (12),

$$\bar{\delta}_s = \alpha_s' - \sqrt{\alpha_s'^2 - 1} \qquad (11)$$

$$\bar{\Delta} = \alpha_s' - \sqrt{\alpha_s'^2 - (1-\bar{a}^2)} \qquad (12).$$

Substituting equations from (5-1) to (7-2) for a equation (2), the magnetic field intensity at a arbitrary point $P(r,\theta)$ can be expressed in (r,θ) coordinate. Thus r and θ components of the field can be written down:

$$\begin{cases} H_r(r,\theta) = -H(r,\theta)\sin(\theta_c - \theta') & (13\text{-}1) \\ H_\theta(r,\theta) = H(r,\theta)\cos(\theta_c - \theta') & (13\text{-}2), \end{cases}$$

where

$$\begin{cases} \sin(\theta_c - \theta') = \dfrac{\xi(\theta')}{\sqrt{1+\xi^2(\theta')}} & (14\text{-}1) \\ \cos(\theta_c - \theta') = \dfrac{1}{\sqrt{1+\xi^2(\theta')}} & (14\text{-}2) \end{cases}$$

$$\xi(\theta') = \frac{\dfrac{1-\bar{r}^2}{2\bar{r}}\sin\theta'}{\alpha_s' - \dfrac{1+\bar{r}^2}{2\bar{r}}\cos\theta'} \qquad (15).$$

2. Sin-cos-probe for a toroidal machine

A sin-cos-probe consists of three coils each of which is wound around a identical toroidal spool. Suppose the number of turns per unit length of the coils is q_s, q_c and q_r, here

$q_c \propto \cos m\theta$: cos-coil

$q_s \propto \sin m\theta$: sin-coil

q_r=constant : reference-coil.

The caluclated values of the outputs of these coils can be obtained by performing the integral $\int_0^{2\pi} H_\theta(\theta) q(\theta)\, d\theta$ in complex domaine for each coil, however there are some complexity in the process to determine Δ and ϕ from the measured signals. This complexity can be avoided by making some modifications of the windings, and a simple treatment becomes possible as well as linear case. It is assumed here that the coils are set near the inner surface of the metal shell. We suppose here m=1. The modification factor $f(\theta)=1-\sigma\cos$, where $\sigma=r_c/R_s$ and r_c is the mean radius of the toroidal spool of the coil. Thus the windings of the coils are as follows:

$$\begin{cases} q_c = q_o f(\theta) \cos\theta, \\ q_s = q_o f(\theta) \sin\theta, \\ q_r = q_{ro} f(\theta), \end{cases}$$

where $q_o=\frac{N_o}{2\pi r_c}$, $q_{ro}=\frac{N_r}{2\pi r_c}$, N_r is total number of turns of the reference coil and N_o is total number of turns of a equivalent Rogowski coil.

3. Design of the probe for TPE-1

3.1 Geometorical requirements

The dimension and the settling feature of our sin-cos-probe are shown in Figs 2 and 3. Fig.3 shows a cross-sectional view on

the equatorial surface of the toroidal metal shell. The probe is to be set in a circular groove with 22 mm in width and 5 mm in depth on the inner surface of the shell. Other measures are as follows: R_s=400, b=63, r_1=56.5, r_2=58.5, r_c=57.5 in millimeter and σ=0.14375.

3.2 Electrical requirements

(1) Withstand voltage is to be greater than 30 KV.

(2) It must be got rid of the effect of strong toroidal magnetic field which may be about thirty times greater than the poroidal field. From these requirements, each coil winding has a insulated gap about 5 mm width at θ=0 for a sin and reference-coil and at $\theta=\pi/2$ for a cos-coil. Both ends of the coil winding wire are brought back through the center of the rectangular cross-section of the spool to the bottom of the coil and led out of the metal shell to an external circuit through a port provided at the bottom of the shell.

(3) Cos-coil signal V_c is to be greater than 0.5 mV after integration under the conditions of I_z=25 KA, $\bar{\Delta}$=0.05 ($\Delta\simeq$3.15 mm) and ϕ=0. Where $V_c \simeq \frac{2lzAN_o}{CRr_c}\bar{\Delta}\ 10^{-7}$ volts (M.K.S), in which CR is a time constant of the integrator and A=wh. This requirement leads to $N_o \geq 1.953\ CR\times 10^4$.

(4) Frequency characteristics wider than from $1KH_z$ to $15\ MH_z$ is desired. The load impedance R_L of the probe is 100 ohm. From this requirement inductance of a coil is to be less than $0.159\ R_L\ T_{min}$ ($\simeq$1.1μH), in which T_{min} is the reciprocal of the maximum frequency in the frequency band. Inductance of Rogowski coil with rectangular cross-section is $L_r=2N_o^2\ w\ \ln\frac{r_2}{r_1}\times 10^{-7} \simeq 2N_o^2\frac{A}{r_c}\times 10^{-7}$. In our case $A=6\times 10^{-6}$ and $L_r \simeq 2.09N_o^2\ 10^{-11}$ Henrry. This leads to $N_r \simeq 2.19\sqrt{L}\times 10^5 \leq 230$.

(5) The signal is to be observable within a error of 1% up to a time corresponding to the time constant of crowbar, which is 150 μsec. This requirement leads to CR≥15 msec and $N_o > 293$. These requirement contend with each other.

4. Determination of the windings

We reduced inevitably the upper limit of frequency band down to 10 MH_z and decided N_r of 272 turns in the first place. However the final value of N_r will be decided after measuring the inductances of the cos and sin-coil to make all of uniform inductance. The roughly estimated inductance L_c of a cos-coil is that $L_c \simeq 1.234\ L_r$, where L_r is inductance of a Rogowski-coil with the same total number of turns as that of a cos-coil. The total number of turns N_c of a cos-coil is $N_c = \frac{2}{\pi} N_o$. Thus we settled on 428 for N_o in expectation of some reduction of inductance by the effect of reversal of the winding sense. However it was found after measurement that this expectation was too optimistic and above rough estimation was rather near the measured value within 10 per cent. The positions of the winding wire at the edges of the spool were given in angle θ to determine the winding of each coil aided by a computer.

5. Acknowledgement

The author wishes to thank Prof. A. Miyahara for offering the valuable informations. Acknowledgement is made to Prof. S. Nagao for a valuable suggestion.

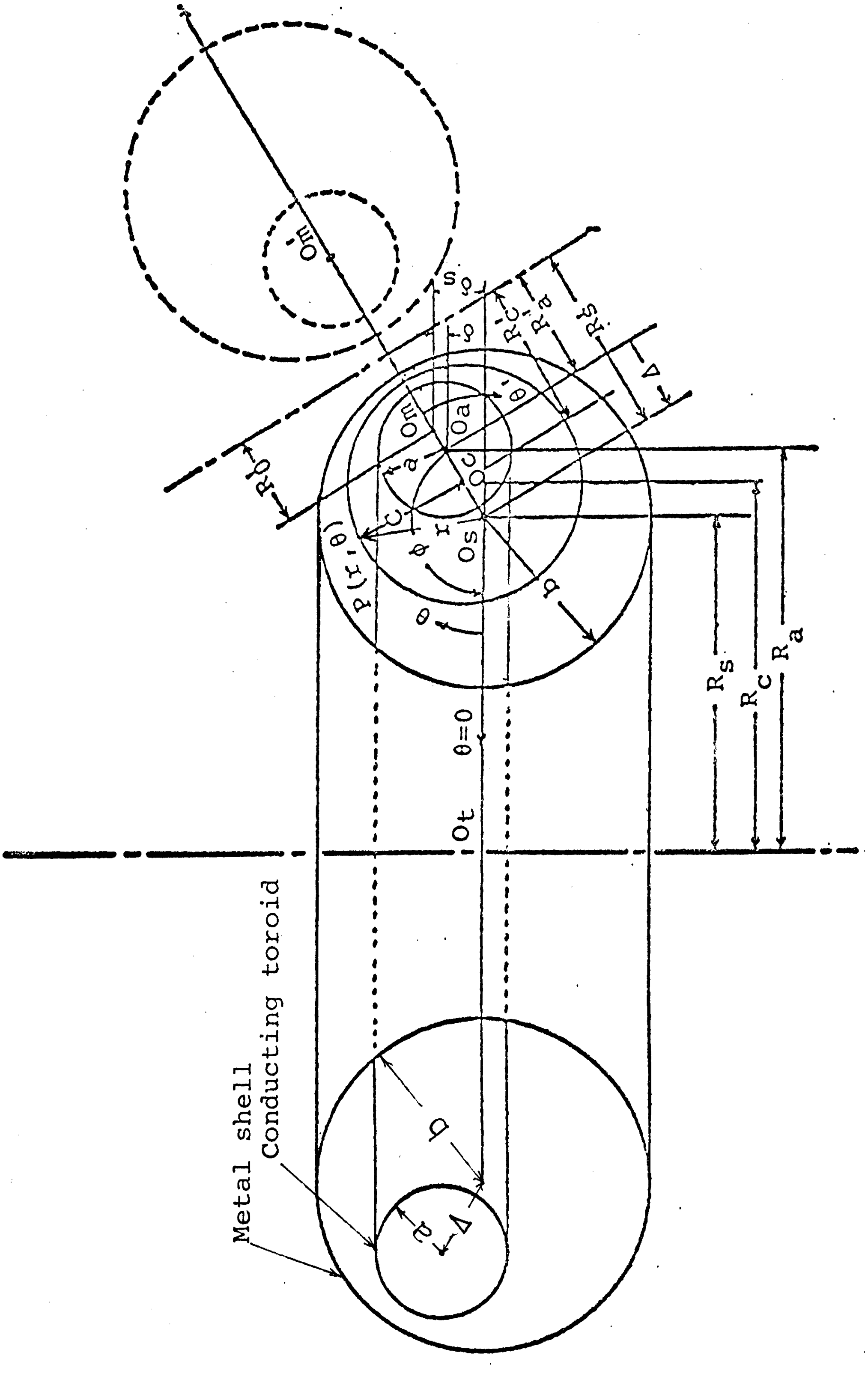
Metal shell
Conducting toroid
Ot
θ=0
P(r,θ)
Os
Oc
Oa
Om
Om'
R_s
R_c
R_a
Δ
b
a
r
θ
θ'
φ

Fig. 1

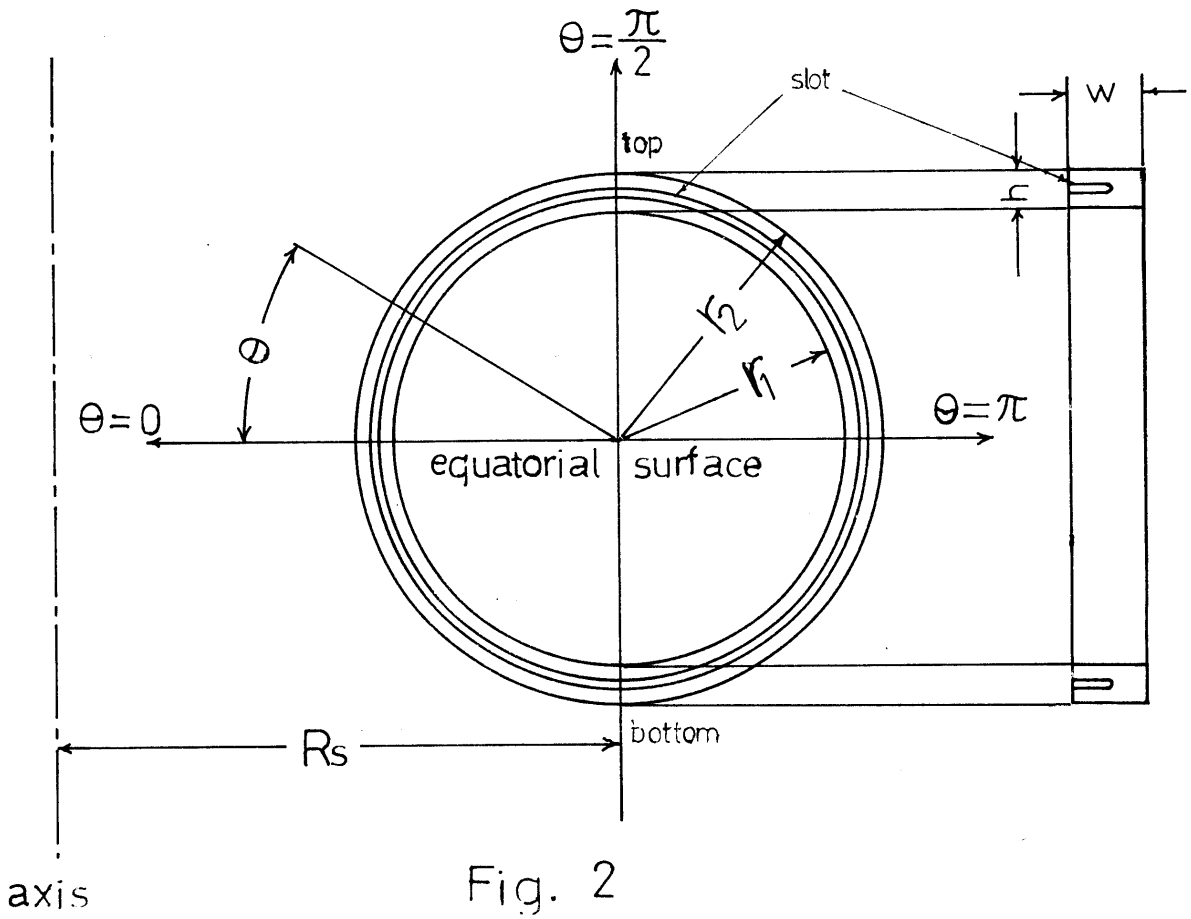
θ=π/2
top
slot
w
t
r2
r1
θ
θ=0
θ=π
equatorial surface
Rs
bottom
axis

Fig. 2

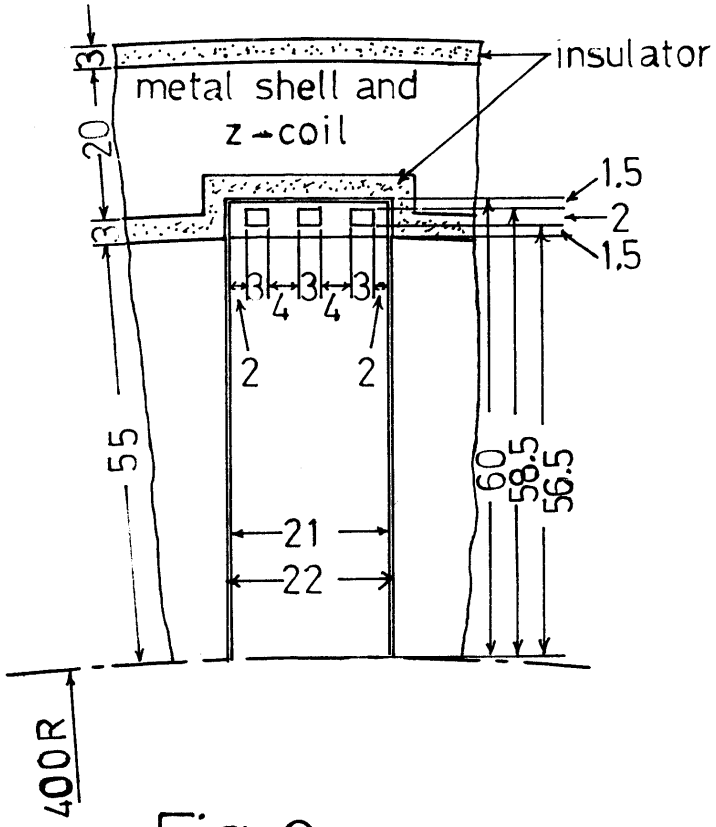
3
insulator
metal shell and
z-coil
20
3
1.5
2
1.5
3
4
3
4
3
2
2
55
60
58.5
56.5
21
22
400R

Fig. 3

LOW FREQUENCY OSCILLATION IN A HIGH DENSITY PLASMA

Yasushi Nishida
Electronic Engineering, Tohoku University, Sendai, Japan
and
Kazushige Ishii
Institute of Plasma Physics, Nagoya University, Nagoya, Japan

Introduction

In a steady state high density plasma with $1 \gg \beta > m/M$, where β is the ratio of material pressure to magnetic pressure, and m and M are the electron and ion mass, respectively, a few investigations have been reported on the Alfvén wave instability in an arc-discharge which have a parallel current along the magnetic field. When the plasma density becomes high, the collisions between the charged particles are strong and the collisional effects must be taken into account.[1] Here, we report the experimental results and its interpretation in a diffused high density plasma without the parallel current. It will be shown that the coupled mode of the collisional Alfvén wave and the collisional drift wave[2] can exist.

Experiments

Experiments were performed on TPD machine of Nagoya Univ. The helium plasma produced by an arc-discharge of the current max. 100 A is diffused through the anode orifice, and has a density $2\times10^{14} \gtrsim n_o \gtrsim 10^{13}$ cm^{-3} in the experimental region with the background neutral pressure of about $6\sim7\times10^{-4}$ Torr. The steady state values and the ion-density fluctuations are measured by the optical probe which is constructed with an optical guide and a photo-multiplier. The optical signal detected is only He-II line intensity. The fluctuating signals are analysed by a real time auto- and cross-correlation method and a

spectrum analyser. Plasma rotation velosity and the plasma density are measured by the Doppler shift of He-II line[3] and CN-laser,[4] respectively.

Magnetic fluctuations are detected by the magnetic probe which, unfortunately, cannot be inserted into the plasma column center as the probe is melted.

Experimental Results

Figure 1 shows the typical examples of the oscillation spectrum. In the region of the maximum density gradient, there exists an about 60 kHz oscillation, which is interested here, while in the column center there exists an about 10 kHz oscillation. In the same figure, the density profile measured by HeII line is also shown, where we assumed that the ion density is proportional to the squre root of the observed relative integrated intensity of HeII line.[3]

The frequency variation on the magnetic field strength is shown in Fig. 2. The frequency changes almost linearly with the magnetic field strength, while the relative amplitude has a peak value near at about 1.5 kG, and decreases gradually with the magnetic field strength. The dispersion relations are shown in Fig.3, which is obtained by the change of the plasma column length. This oscillation disappears at $k_{\parallel} \approx 0.065$. In this experiment, it is found that the half wave length can be determined by the length between anode and target.

Discussion

Interpretation of this instability is tried as the coupled mode of collisional Alfvén instability and the collisional drift mode. By starting with the ion and electron fluids equations with ion viscosity across, and electron collision along the magnetic field, we finally obtained the next dispersion relation.

$$\frac{2b}{t_{\parallel}(V_A^2 K_{\parallel}^2 b)}\omega^3 + \left[ib + i\left(\frac{1+2b}{t_{\parallel}} + \frac{2}{t_{\perp}}\right)\frac{1}{t_{\parallel}(V_A^2 K_{\parallel}^2 b)} + \frac{\omega_*}{t_{\parallel} V_A^2 K_{\parallel}^2}\right]\omega^2 - \left[\left(\frac{1+2b}{t_{\parallel}} + \frac{1}{t_{\perp}}\right) + \frac{2}{t_{\perp} t_{\parallel}}\frac{1}{t_{\parallel}(V_A^2 K_{\parallel}^2 b)}\right.$$

$$- i\omega_* \left\{ b + \left(\frac{2}{t_\perp} - \frac{1}{t_\parallel}\right) \frac{1}{t_\parallel (V_A^2 K_\parallel^2 b)} \right\} \Big] \omega$$

$$+ \left(\frac{1}{t_\parallel} - \frac{1}{t_\perp}\right) \omega_* - \frac{2i}{t_\perp t_\parallel} = 0, \qquad (1)$$

Here, we assumed $E = -\nabla\varphi - (1/c)\partial A/\partial t \cdot \hat{z}$, and $\beta \ll 1$, where $b = \rho_i^2 k_\perp^2/2$, $1/t_\parallel = kTk_\parallel^2/m\nu_{ei}$, $1/t_\perp = b^2\nu_{ii}/4$, V_A the Alfvén velocity and ω_* is the drift angular frequency caused by density gradient. Other notations are standard.

Examples of numerical values are shown in Fig. 3, which are obtained by the use of experimental values. Examples of more wide variations of numerical values are shown in Fig. 4. We can see in Fig. 4 that the collisional mode is different from the collisionless mode obtained earier.[5]

In Fig. 3, the ion rotaion around the axis[6] is not corrected. If it is done, the experimental values will be changed a little. The observed mode is rather collisional drift wave branch than the collisional Alfvén wave as seen in Fig. 3. The precise investigation is now undertaken.

Authors are gratefull to Mr. A. Ogata for his measurement of cross- and auto-correlation.

References

1 L.C.Woods, Phys. Fluids 6, 729 (1963).

2 H.W.Hendel, T.K.Chu, and P.A.Politzer, Phys. Fluids II, 2426 (1968).

3 M.Ohtzuka (private communication).

4 A.Nishizawa (private communication).

5 B.B. Kadomtsev, Plasma Turbulence (Academic Press, London, 1965) p.78.

6 M.Ohtzuka (private communication).

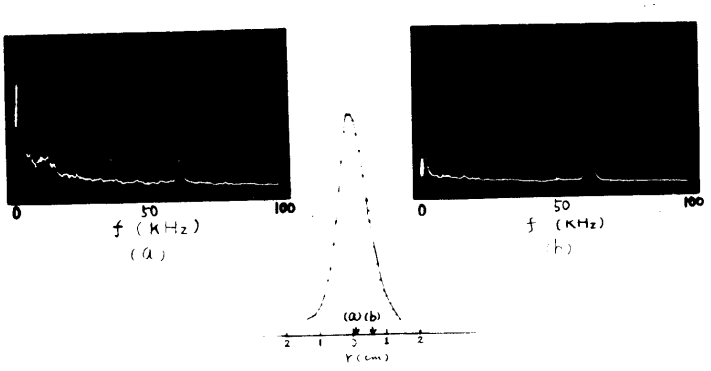

Fig.1 Instability spectrum and the ion density profile.

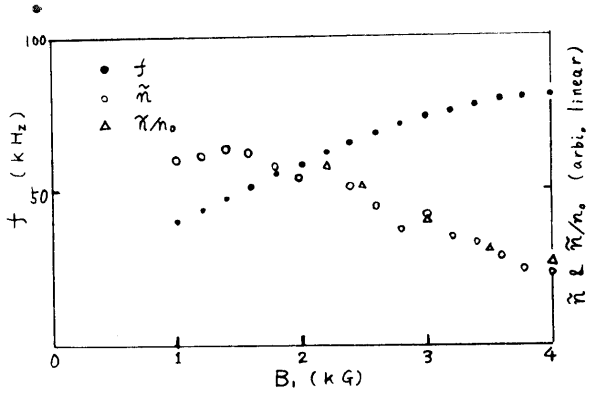

Fig.2 Instability frequency and amplitude vs. the magnetic field.

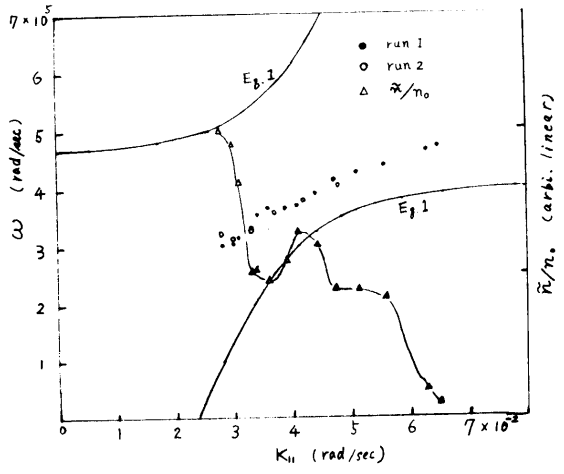

Fig.3 Dispersion relations. Solid lines are the real part obtained from Eq.1.

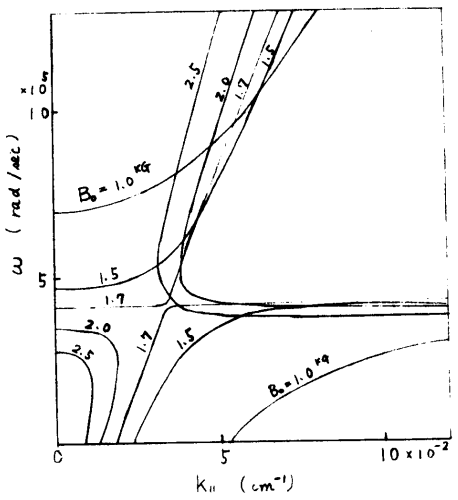

Fig.4 Dispersion relation calculated from Eq.1.

Distribution Measurement in $\mathbb{k}$-Space of Ion Acoustic Wave by Microwave Scattering

Atsushi Mase, Takumi Yamamoto
and Takashige Tsukishima

Faculty of Engineering, Nagoya University, Nagoya

The importance of using incoherent scattering of electromagnetic waves from plasmas as a diagnostic tool has been widely recognized. Microwave scattering from a variety of laboratry plasmas have been observed.

We report here on the experimental results of microwave scattering from ion acoustic wave excited externally in a mercury positive column, with emphasis on the measurement of the intensity distribution of the ion acoustic wave in the wave vector ($\mathbb{k}$) space.

A schematic of the experimental setup is shown in Fig. 1. The plasma is produced in a glass tube with 5 cm i.d. and 40 cm long. The ion acoustic wave is excited via the asterisk grid, to which an AC signal of frequency ω from an oscillator is applied. The grid is located 16 cm distant from the cathode. A microwave of the frequency $\omega_i/2\pi$ = 35 GHz is launched through the transmitter horn and focused on the discharge tube, using a dielectric lens. The transverse width of the incident beam is about 2 cm on the tube axis, while the intensity is nearly constant along the beam direction over the tube diameter. The electric field vector

E_i is perpendicular to the tube axis. Both the discharge tube and the receiver horn are made rotatable around an axis paralell to E_i, located at the center of the tube. The plasma column is in the far field of the horns. The scattered signal picked up by the receiver horn is detected by a homodyne system. In order to obtain a good signal to noise ratio at the receiver output, a frequency based correlator[2] with 3 kHz i.f. band width is used.

For the present experimental condition, $\omega_i \gg \omega$, the scattered waves with frequencies $\omega_s = \omega_i + \omega$ and $\omega_s' = \omega_i - \omega$, the incident wave and the local oscillator wave enter into the crystal detector together. Their electric field amplitudes are described as E_s, E_s', E_i and E_l respectively. Then the outputs of the two crystals in Fig.1 are given by,

$$\begin{aligned} e_A &= A\,[\,E_s\cos(\omega_s t+\varphi_s)+E_s'\cos(\omega_s' t+\varphi_s') \\ &\quad +E_l\cos(\omega_i t+\varphi_l)+E_i\cos(\omega_i t+\varphi_i)\,]^2 \\ e_B &= B\,[\,E_s\cos(\omega_s t+\varphi_s)+E_s'\cos(\omega_s' t+\varphi_s') \\ &\quad -E_l\cos(\omega_i t+\varphi_l)+E_i\cos(\omega_i t+\varphi_i)\,]^2\,, \end{aligned} \qquad \ldots\ldots(1)$$

when the square characteristic is assumed for the crystals. In eq. (1), A and B are the conversion gain factor of the crystals, and φ_s, φ_s', φ_l and φ_i are the phase components of the each electric field. The i.f. outputs of frequency ω are given by,

$$e_A' = A'[\, E_s E_1 \cos(\omega t + \varphi_s - \varphi_1) + E_s' E_1 \cos(\omega t + \varphi_1 - \varphi_s')$$
$$+ E_s E_i \cos(\omega t + \varphi_s - \varphi_i) + E_s' E_i \cos(\omega t + \varphi_i - \varphi_s')\,]$$

$$e_B' = B'[\, E_s E_1 \cos(\omega t + \varphi_s - \varphi_1) + E_s' E_1 \cos(\omega t + \varphi_1 - \varphi_s')$$
$$- E_s E_i \cos(\omega t + \varphi_s - \varphi_i) - E_s' E_i \cos(\omega t + \varphi_i - \varphi_s')\,] \quad \cdots\cdots (2)$$

where A' and B' are the constants. When the condition $E_1 \gg E_i$ is satisfied, we obtain the following correlator output P_r,

$$P_r = \overline{|e_A \times e_B|} = \frac{A'B'}{2} E_1^2 \,(E_s^2 + E_s'^2 + 2E_s E_s' \cos\phi\,), \cdots\cdots (3)$$

where upper bar denotes the time average, and $\phi = \varphi_s + \varphi_s' - 2\varphi_1$. The value of ϕ can be controlled by a phase shifter inserted next to the receiver horn. Note that P_r becomes independent of ϕ when only either of the two satellites are to be received. The corresponding matching conditions for the wave vectors are given by $\mathbb{K}_s = \mathbb{K}_i + \mathbb{k}$ and $\mathbb{K}_s' = \mathbb{K}_i - \mathbb{k}$ respectively, where $K_s = \omega_s/c$ and $K_s' = \omega_s'/c$, c is the light velocity. When $K_i \simeq K_s \simeq K_s'$, the matching conditions can be expressed as $k = 2K_i \sin(\theta_s/2)$, where θ_s is the scattering angle, i.e., $\cos\theta_s = \mathbb{K}_i \cdot \mathbb{K}_s / K_i K_s$.

Figure 2 shows the observed P_r versus θ_s, for the normal incidence to the tube axis. The vertical bars indicate the variations of P_r when ϕ is varied from 0 to 2π rad. at each θ_s. The similar measurements were repeated for varying ω

from 20 kHz to 60 kHz. The k values calculated from the θ_s corresponding to the peaks satisfy the dispersion relation, $\omega = kC_s$, where C_s is found to be independent of the wave amplitude, and has a value of the ion acoustic velocity, thus the effect of the ballistic mode may be small. The broadening of the each peaks in Fig.2 is identified as due to the finite beam width. Refering to Eq.(3), it may be then concluded that the peaks for $\theta_s > 0$ and $\theta_s < 0$ are due to E_s and E_s' respectively, and that they are scattered by the ion waves propagating at the angle $\theta_s/2$ with respect to the tube axis.

Then, to see the intensity distribution of the ion acoustic wave as a function of the zenithal angle α as measured from the tube axis, the discharge tube is rotated while the receiver horn is located at the fixed θ_s giving the peak P_r for the normal incidence. The results are shown in Fig.3 (a), (b). It is seen that the wave intensity shows the maximum at $\alpha = 0$, as is expected. The observed angular spread for f = 30 kHz is wider than that for f = 40 kHz, and both exceed the instrumental broadening.

In Fig.4 is plotted the scattered power by the wave with $\alpha = 0$ as a function of the illuminating position as measured from the exciting grid toward the anode. It is seen that the wave attenuates as it propagates toward the anode. The attenuation is heavy and exponential for f = 30 kHz. With increasing frequency the attenuation constant decreases. For

$f \geqq 50$ kHz an amplitude oscillation-like phenomenon is observed instead of the simple exponential attenuation. This might be due to some nonlinear effects. It is interesting to note that the heavier attenuation is accompanied with the wider angular spread in k-space.

This work is supported in part by the collaborating research program at Institute of Plasma Physics, Nagoya University, and also by the Grant-in-Aid for Scientific Researches of the Ministry of Education.

References

1) V. Arunasalam, M. A. Heald, and J. Sinnis: Phys. Fluids 14, 1194 (1971).

L. D. Bollinger and H. Bohmer: Phys. Fluids 15, 693 (1972).

2) T. Tsukishima and N. Iwama: IPPJ-DT-16, Inst. of Plasma Phys., Nagoya, Mar. 1970.

Figure Captions

Fig.1. Schematic diagram of the experimental setup.

Fig.2. Received power versus scattering angle.

Fig.3. Intensity of ion acoustic wave versus zenithal angle α from the tube axis. (a) f = 30 kHz, (b) f = 40 kHz The incident beam illuminates the region 3.5 cm distant from the exciting grid. The directional vector with α =0 points to the anode.

Fig.4. Scatterd powers by the wave with α =0 versus the illuminating position as measured from the exciting grid toward the anode.

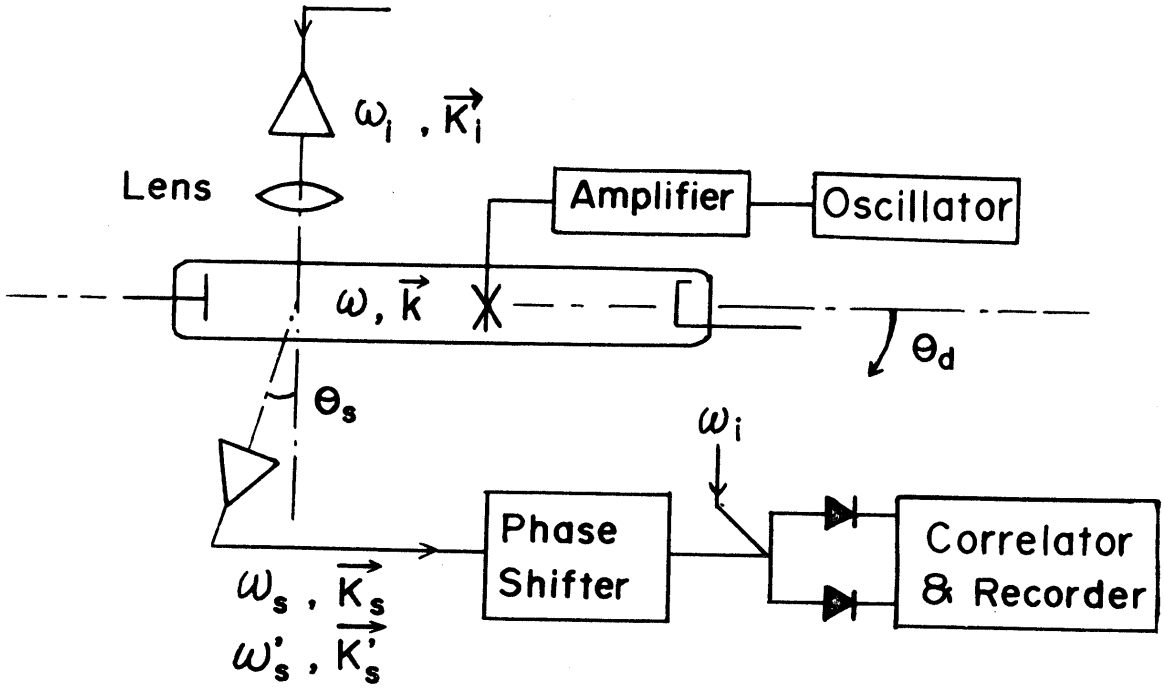
ω_i , $\vec{K_i}$
Lens
Amplifier
Oscillator
ω, $\vec{k}$
Θ_d
Θ_s
ω_i
Phase Shifter
Correlator & Recorder
ω_s , $\vec{K_s}$
ω_s' , $\vec{K_s'}$

Fig. 1

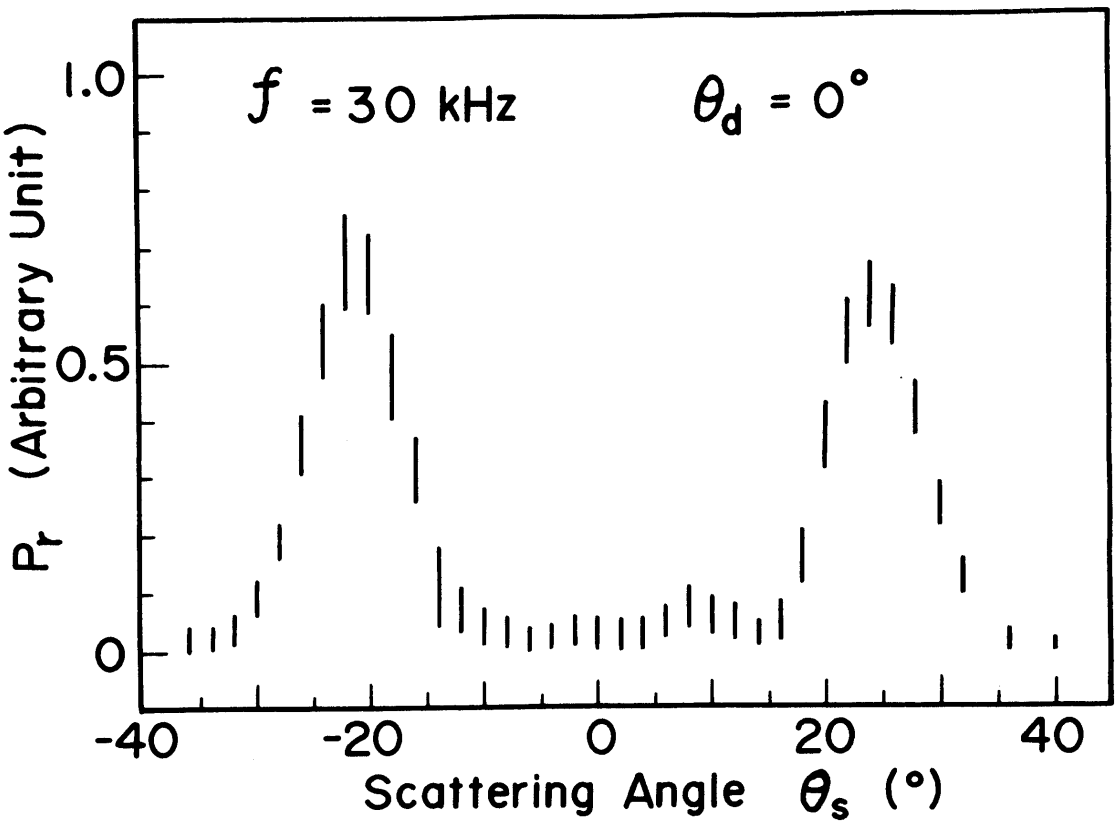
f = 30 kHz
θd = 0°
1.0
0.5
0
Pr (Arbitrary Unit)
-40
-20
0
20
40
Scattering Angle θs (°)

Fig. 2

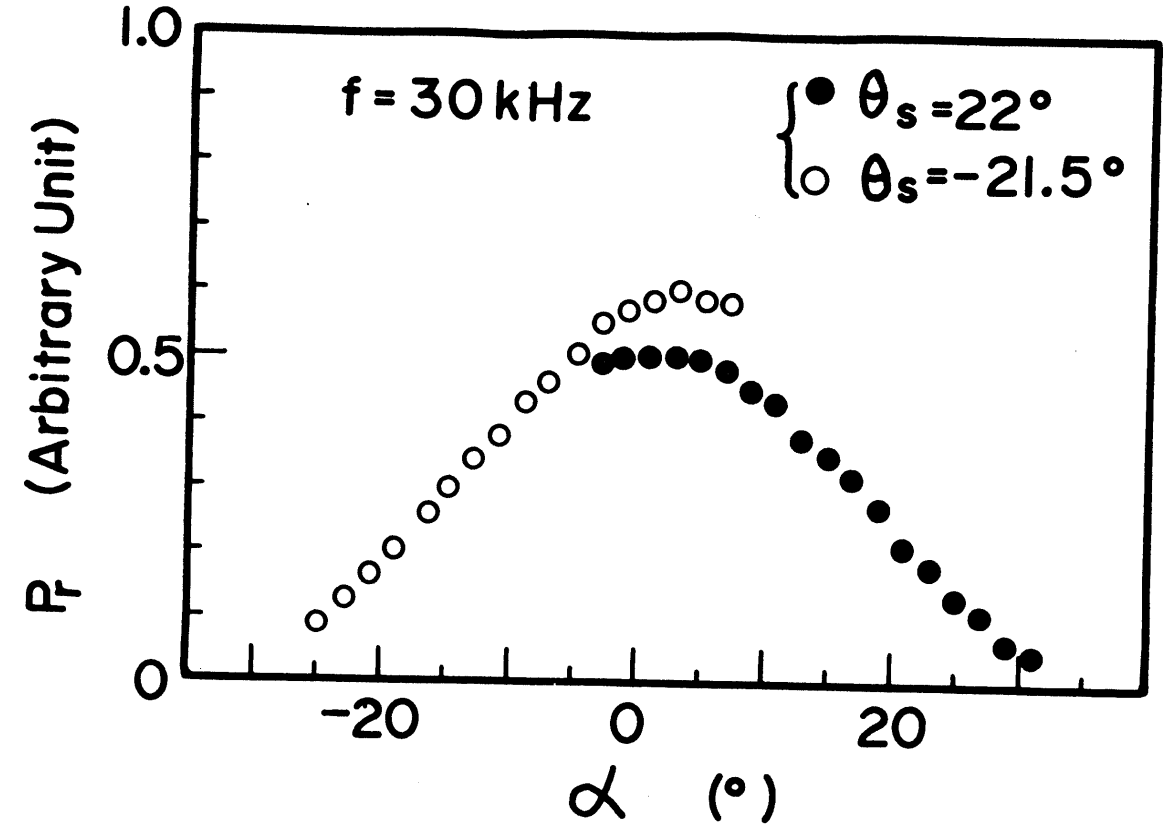
1.0
0.5
0
f = 30 kHz
θs = 22°
θs = -21.5°
Pr (Arbitrary Unit)
-20
0
20
α (°)

(a)

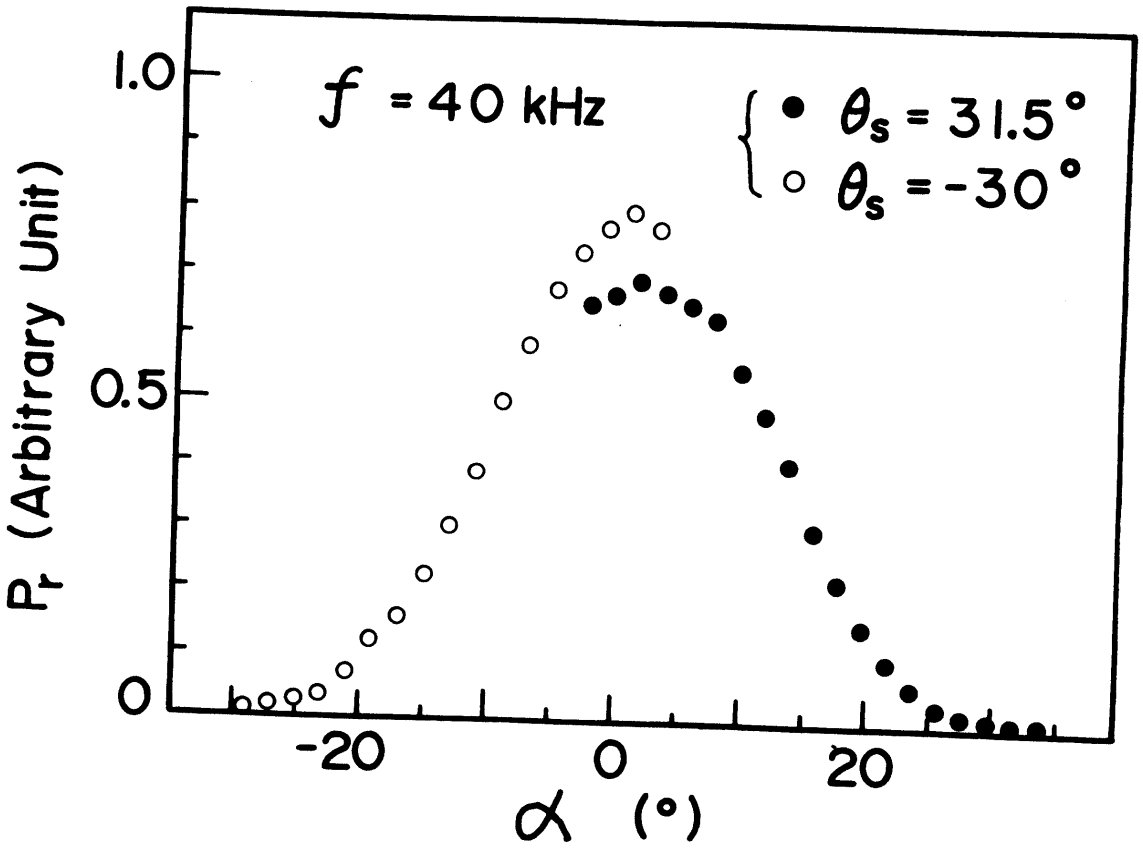
1.0
0.5
0
f = 40 kHz
θs = 31.5°
θs = -30°
Pr (Arbitrary Unit)
-20
0
20
α (°)

(b)

Fig. 3

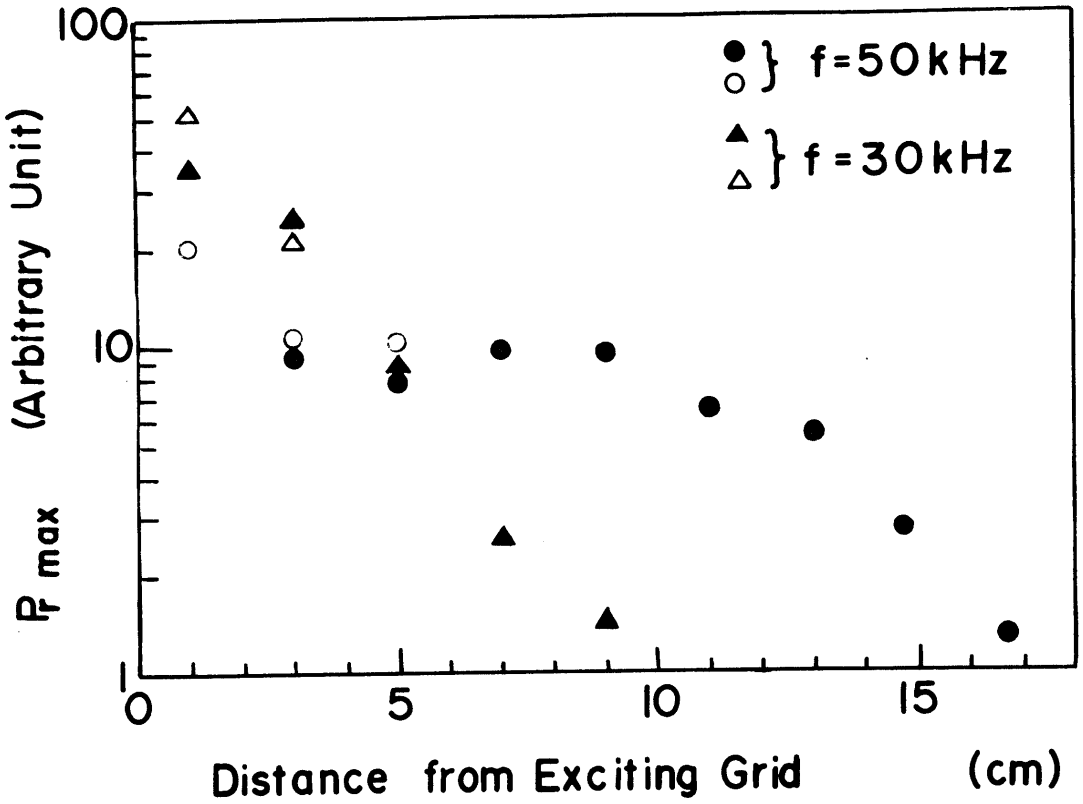
100
10
1
0
5
10
15
$P_{f\,max}$ (Arbitrary Unit)
f=50kHz
f=30kHz
Distance from Exciting Grid (cm)

Fig. 4

Review of Particle Diagnostics

N. Inoue

Department of Nuclear Engineering,

Faculty of Engineering, University of Tokyo

A variety of corpuscular measurements have been developed for the diagnostics of hot plasmas.[1)-3)] The particle measurements can be divided into two categories: mass and energy analysis of particles emitted from plasmas and methods of beam probing. In the latter case one injects particle beams into the plasma and observe the interaction between the beam particles and the plasma particles. In this review we treat the particle measurements which are applicable to the closed magnetic confinement system.

A) Measurement of particles emitted from the plasma

1. neutral particle

Fast neutral particles produced by the charge exchange reactions between the plasma ions and the residual gas come out of the system across the confining field. Mass and energy analysis of such neutrals offer the informations about the energy distribution (in the most cases, about the temperature) and the ion species of the plasma. The particle loss rate by charge-exchange is estimated from the absolute intensity of the emitted neutrals. Figure 1 shows the apparatus of measurement which has been applied to a toroidal pinch devices.[4)] For the Maxwellian plasma the detector current resulting from the ions with the energy of from W to W+ΔW is given by

$$\Delta J(W) = A\sigma_i(W)\sigma_{cE}(W)W^{5/2}\exp(-W/kT_i), \qquad (1)$$

where A is constant, $\sigma_i(W)$ is the ionization cross section of neutrals in the stripping cell, $\sigma_{cE}(W)$ is the charge exchange cross section in the plasma, and kT_i is the ion temperature.

The ion temperature is deduced from the inclination of plot of $\log\{\Delta J/(\sigma_i \sigma_{cE} W^{5/2})\}$ vs W.

2. charged particles

Since the trajectories of charged particles emanating from the plasma across the confining field is much complicated, it is usually different to relate the experimental results to the plasma parameters. The measurement may be fruitful if the observed results are interpretable by the recently developed diffusion theory of toroidal plasma.[5] In that case it is necessary to analyze and detect the charged particles at the plasma surface. Several types of the analyzer and the detectors have been developed for such applications.[6)-9)]

3. nuclear reaction products

Nuclear reaction rate in a hot plasma is given by

$$R = n_1 n_2 \int f(\vec{v}_1) f(\vec{v}_2) |\vec{v}_1 - \vec{v}_2| \sigma(|\vec{v}_1 - \vec{v}_2|) d\vec{v}_1 d\vec{v}_2. \qquad (2)$$

For the Maxwellian deuterium plasma, this comes to[10]

$$R_{DD} = \frac{n_D^2}{2} 260 \times 10^{-16} (kT_i)^{-3/2} \exp\left[-\frac{18.76}{(kT_i)^{1/3}}\right], \qquad (3)$$

where R, n, and kT_i are in units of $m^{-3}s^{-1}$, m^{-3}, and keV, respectively. We can estimate the ion temperature from the observed total neutron yield, if the plasma density is known. It should be noticed that the reaction rate is much sensitive to the high energy part of the energy distribution and the deviation of the distribution from the Maxwellian leads to a large error. When the neutron production is not due to the thermonuclear origin but due to anomalously accelerated ions, the emission of neutron occurs anisotropically.

B) Beam probe

1. neutral particle beam

When the neutral particle beam traverses across the plasma,

it is predominantly attenuated by charge exchange reactions and electron-impact ionizations. Beam intensity after transmission of the plasma with the thickness of L and the density n is given by

$$I = Io \exp\left\{-nL\left(\sigma_{cx} + \frac{\langle\sigma_i v\rangle}{v_B}\right)\right\} , \qquad (4)$$

where I_0 is the initial intensity of the beam, v_B is beam velocity, σ_{cx} is the charge exchange cross section and $\langle\sigma_i v\rangle$ is the product of the electron impact ionization cross section and the relative velocity between the beam and the plasma electrons averaged over the electron velocity distribution. By selecting the beam species and energy, one can measure the several kinds of plasma parameters and cover wide range.[11)-14)] Figure 2 shows a beam probe system used for the measurement of ion density.

2. heavy-ion beam-probe

Heavy-ion beam-probe technic has been developed for the measurement of ST TOKAMAK plasma.[15)] The apparatus of the measurement system is shown in Fig.3. Singly ionized thalium beam is injected into the plasma region where they are ionized by electron impact ionization. The intensity and the energy of doubly ionized ions gives the electron density and the plasma space potential, respectively. The toroidal current distribution can also be obtained by measuring the deviation of the thalium beam from its original path. The measurement of current distributions by a high energy alpha particle beam is now under investigation in JFT-2 TOKAMAK.[16)]

3. electron beam probe

Electron beam has been used for the measurement of space potential and the trace of magnetic field. For the latter use[17)] a pulsed electron beam is injected along the magnetic lines of force by an electron gun with 2 mm outer diameter, and detected

with a small sized probe (0.5 mm in diameter). The magnetic surface and the rotational transform angle of a stellarator field is directly obtained by this method.

Reference

1) V. V. Afrosimov and I. G. Gladkovskii: Soviet Physics-Technical Physics, 12(1966)1135.

2) J. E. Osher: Plasma Diagnostic Technics, ed. R. H. Huddlestone and L. L. Stanley (Academic press N. Y. 1955) Chap.12, p.517.

3) H. W. Drawin: Plasma Diagnostics, ed.W. Lochte Holtgreven (North-Holland 1968) Chap.13.

4) N. Noda, K. Sato, R. Akiyama, N. Inoue and T. Uchida: Nuclear Fusion, 12(1972)607.

5) B. B. Kadomtsev and O. P. Pogutse: Nuclear Fusion, 11(1970)67.

6) M. S. Ioffe, R. I. Sobolev, V. G. Tel'kovskii and E. E. Yushmanov: Soviet Physics-JETP, 12(1961)1117.

7) E. I. Dobrokhotov and I. N. Moskalev: Soviet Physics-Technical Physics, 15(1970)808.

8) C. W. Erickson: Rev.sci.Instrum. 37(1966)1308.

9) C. W. Erickson: Phys.of Fluids, 13(1970)819.

10) D. J. Rose and M. Clark Jr.: Plasmas and Controlled Fusion (MIT press. N. Y. 1961) p.80.

11) V. V. Afrosimov, B. A. Ivanov, A. I. Kislyakov and M. P. Petrov: Soviet Physics-Technical Physics, 11(1966)63.

12) H. P. Eubank, P. Noll and F. Tappert: Nuclear Fusion, 4(1964)312.

13) N. Inoue: Japan J.of Phys.Soc., 32(1972)1095.

14) V. A. Finlayson, F. H. Coensgen and W. E. Nexsen, Jr.: Nuclear Fusion, 12(1972)659.

15) R. L. Hickock and F. C. Jobes: AFOSR TR-72-0018.

16) S. Kawasaki and K. Inoue: Nuclear Fusion, 12(1972)387.

17) E. Berkl, G. v. Gierke and G. Grieger: IPP 2/69(1968).

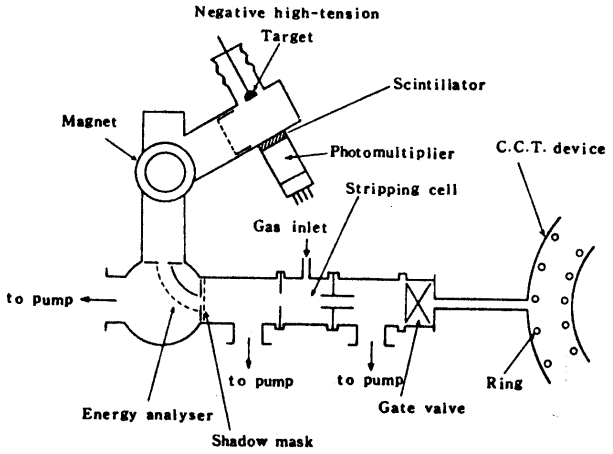

FIG. 1. Diagram of apparatus for investigating neutral particles emitted from the plasma of the C.C.T. device.

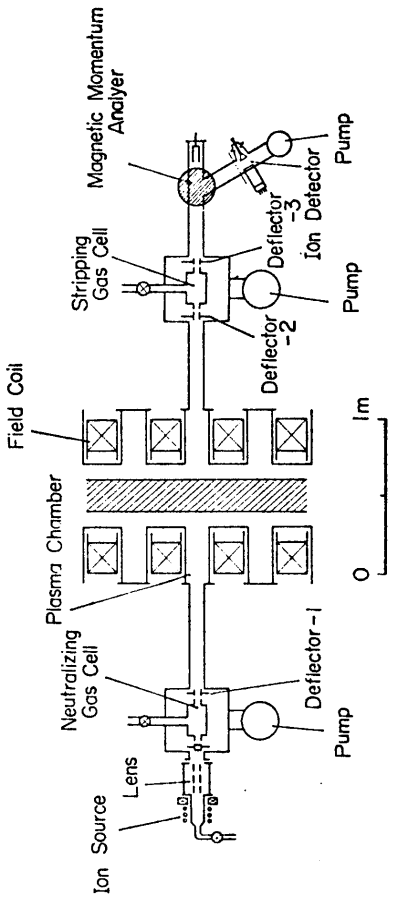

Fig. 2. Beam probing system for gas beams.

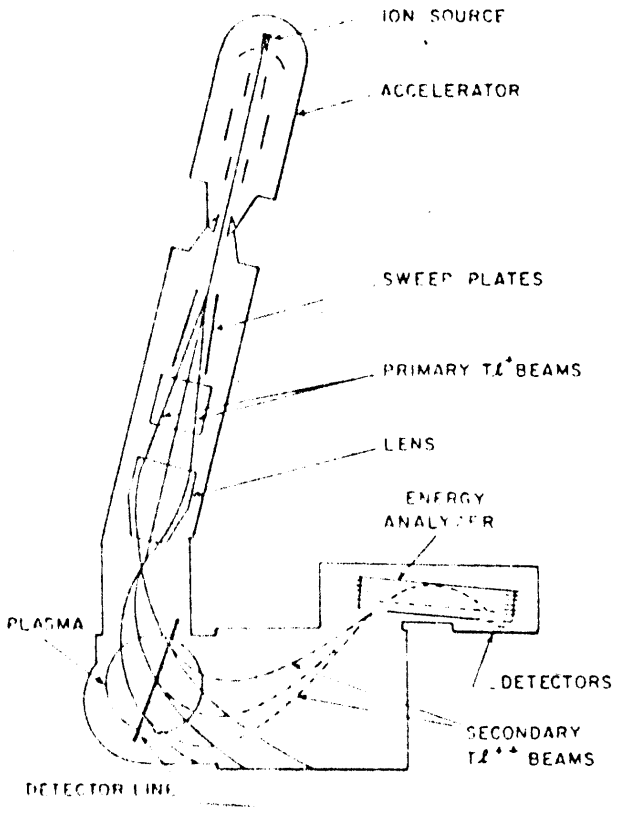
ION SOURCE
ACCELERATOR
SWEEP PLATES
PRIMARY Tℓ⁺ BEAMS
LENS
ENERGY
ANALYZER
PLASMA
DETECTORS
SECONDARY
Tℓ⁺⁺ BEAMS
DETECTOR LINE

Fig.3

Calibration of Electron Bombardment Detector for Fast Neutral Particles

Hajime ISHIMARU and Kohtaro SATOH

Department of Physics, Faculty of Science,

University of Tokyo, Tokyo,

Abstract

An electron bombardment detector for fast neutral particles has been accomplished and calibrated for time-of-flight energy analyzer of plasma diagnostics. The ion output is proportional to the incident number of neutral particles at the range of $10^7 \sim 10^{10}$ particles/sec. Overall detection efficiency of the system for thermal hydrogen is $\eta \sim 0.5$. Response time of the detector is 5×10^{-6} sec.

SPECTRAL LINE PROFILE AND ITS APPLICATION TO PLASMA DIAGNOSTICS

Toshiatsu Oda

Department of Physics, Hiroshima University, Hiroshima

The profile of a spectral line from plasma leads us to know the important properties of the plasma. In the most laboratory plasma, Doppler and Stark effect are the dominant broadening mechanisms of the spectral line.

In this short article, emphasis is put on some examples of the recent results of the research for the shape of the spectral line due to Doppler and / or Stark effect. The latest review of the spectral line profile is given by Mori[1)] who also discusses many topics in the plasma spectroscopy.

DOPPLER EFFECT

Doppler broadening directly comes from the motion of the radiating atoms (ions) in plasma, so that the ion temperature or the velocity distribution of the ion may be obtained by measuring the line profile although other broadening mechanisms, e.g. Stark broadening, should be taken into account. This method, however, is not applicable to a sufficiently high temperature plasma because it almostly consists of bare nuclei and electrons. Even in this case, the Doppler broadening measurement is still possible if one put small amount of the neutral atoms into the plasma

and make a hot ion exchange its charge with the injected atom in the plasma. An example of such measurement is shown in Fig.1.

There is one more problem for the Doppler broadening measurement, that is, additional Doppler effect due to the plasma mass motions which generally exist in plasmas. For an extensive discussion of this problem, the reader is refered to a recent review article by Kaufman[3]. Here we only present a result of the Doppler broadening measurement for the plasma of turbulent heating experiment[4),5)] which was carried out on the BSG II device under the collaborating research program at the Institute of Plasma Physics, Nagoya University. In Fig.2 is shown the typical development and decay of the profile of the helium ion line (He II 4686 Å) during the heating process[5]. It appears that the line profile at the early stage of the heating process is fairly well shaped like the Gaussian, but it becomes complicated shape (consists of more than two components) with development of the process. This may suggest that mass motions exist locally in the plasma ($v \sim 10^6$ cm/s).

STARK EFFECT

Stark broadening of the spectral line from plasma is usually dominated by the charged particle-produced field and also by the oscillating field originating from various waves in plasmas. The latter field in the turbulent plasmas has been recently investigated along the line of Stark effect

and it has been shown that this method leads one to powerfull information for the transport phenomena and heating in the turbulent plasmas.

As is well known, Stark-broadened spectral lines by the charged particle field have been widely used as a convienent contactless probe for the plasma density. Balmer series lines of hydrogen[6], helium lines[7], and ionized helium lines[8] have been investigated in detail and so these lines are very convienent for the density measurement.

High frequency strong electric fields influence the radiating lines for producing the satellite lines through more than one quantum process. It was on He I lines that the first experiment[9] of the satellite lines was performed. For not so strong field of high frequency, the second order perturbation theory[10] for a two quantum process is valid (see Fig.3). In this case, the ratio of the intensity of the satellite line to that of the allowed line gives one the oscillating field strength and the separation of the satellite from the forebidden line the frequency, ω, of the field. For strong field where the perturbation is not valid, it has been pointed out[11] that pattern of the satellite becomes very complicated as shown in Fig.4. Simillar satellites have been found on the Balmer lines of hydrogen[12].

The low frequency fields due to ion-acoustic turbulence also make a spectral line broad and shifted[13]. For hydrogen lines, the average intensity of the field is approximately given by

$$\langle \hat{E}^2 \rangle^{1/2} \simeq \frac{8\pi\, c\Delta\lambda_{1/2}}{3(n^2 - n'^2)ea_0\lambda_0^2}$$

where $\Delta\lambda_{1/2}$ is the measured half width, λ_0 the wavelength of the line center, a_0 the Bohr's radius, and n and n' are the quantum number of upper and lower levels, respectively.

The above described diagnostic methods have a disadvantage that light is collected only along the line of sight through the plasma, i.e. spatial resolution of the measurements are not well available. Recently, it has been shown that the light scattering techniques by using tunable dye laser can be applied to this problem which make the local measurement possible[14].

REFERENCES

1) K. Mori: Bunko Kenkyu 20 (1971) 1(in Japanese).

2) S. V. Mirnov and I. b. Semyonov: Atomnaya Energiya 28 (1970) 129.

3) A. S. Kaufman: "Advances in Atomic and Molecular Physics Vol 6" (D. R. Bates ed., Academic Press, New York 1970).

4) K. Adati, T. Kawabe, T. Oda, Y. Takezaki, T. Yokota, T. Uyama and K. Watanabe: Phys. Rev. Letters 29 (1972) 1223.

5) Ann. Rev. I. P. P. Japan, Nagoya Univ. (1971 - 1972) 63 and Ann. Rev. I. P. P. Japan, Nagoya Univ. (1972 - 1973) to be issued.

6) R. A. Hill, J. B. Gerardo and Paul C. Kepple: Phys. Rev. A3 (1971) 855.

7) J. R. Greig and L. A. Jones: Phys. Rev. A1 (1970) 1261.

8) L. A. Jones, J. R. Greig. T. Oda and Hans R. Griem: Phys. Rev. A4 (1971) 833.

9) H.-J. Kunze and H. R. Griem: Phys. Rev. Letters 21 (1968) 1048.

10) W. S. Cooper III and H. Ringler: Phys. Rev. 179 (1969) 226.

11) W. W. Hicks. R. A. Hess and W. S. Cooper: Phys. Rev. A5 (1972) 490.

12) C. C. Gallagher and Morton A. Levine: Phys. Rev. Letters 19 (1973) 897.

13) G. V. Sholin: Sov. Phys. - Dokl. 15 (1971) 1040.

14) C. F. Burrell and H.-J. Junze: Phys. Rev. Letters 29 (1972) 1445.

FIGURE CAPTIONS

Fig. 1. Spectral line profiles of H_α and D_α lines from the deuterium plasma in Tokamak T - 3[2] where cold hydrogen gas is injected into the plasma about 10 msec. after the discharge.

Fig. 2. Temporal variation of He II 4686 Å line profile. The initial plasma temperature and density are $T \sim 2$ eV and $n \sim 5 \times 10^{13}$ cm^{-3}, respectively.

Fig. 3. Partial energy level diagram and the spectrum in the vicinity of the allowed line (A). Transition from level j to k is allowed, but one from i to k is forbidden. Levels v_+ and v_- indicate virtual levels. S and F indicate satellite lines and forbidden line, respectively.

Fig. 4. Calculated Stark profiles of He I 4922 Å line for the case of a linearly polarized electric field. Each profile is the result of folding the theoretical line profile with an instrument function of FWHM of 0.2 Å. A double arrow in the figure shows a single decade in logarithmical scale.

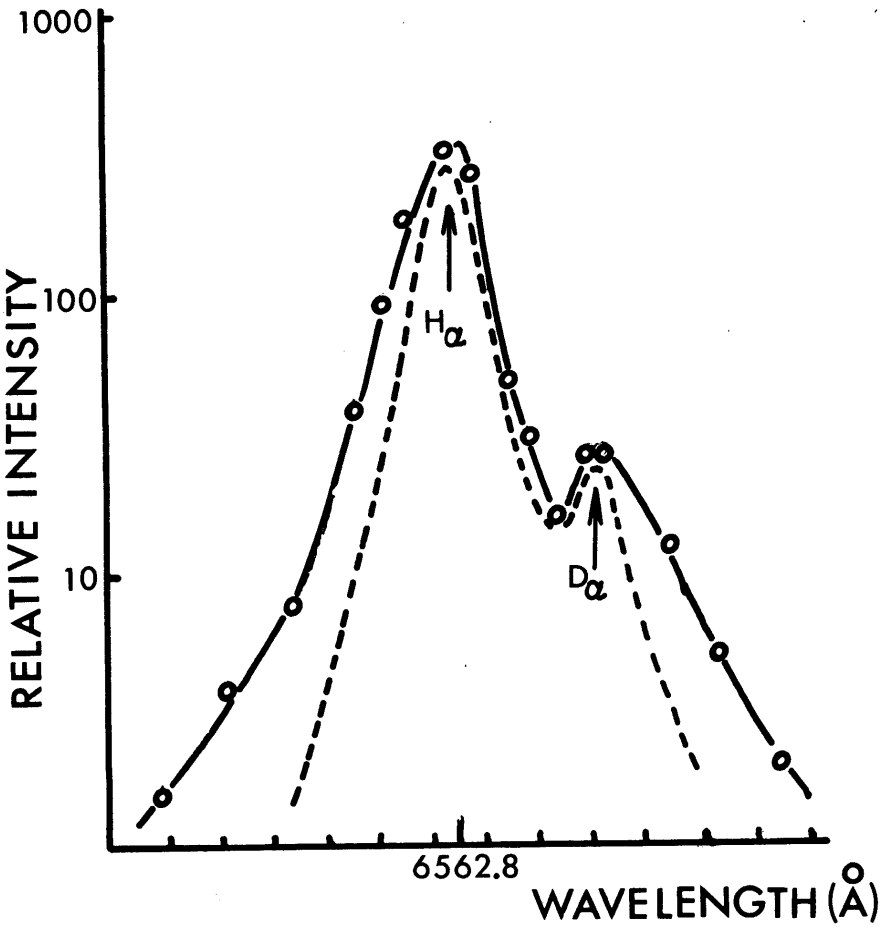
1000
100
10
RELATIVE INTENSITY
H_α
D_α
6562.8
WAVELENGTH (Å)

Fig. 1.

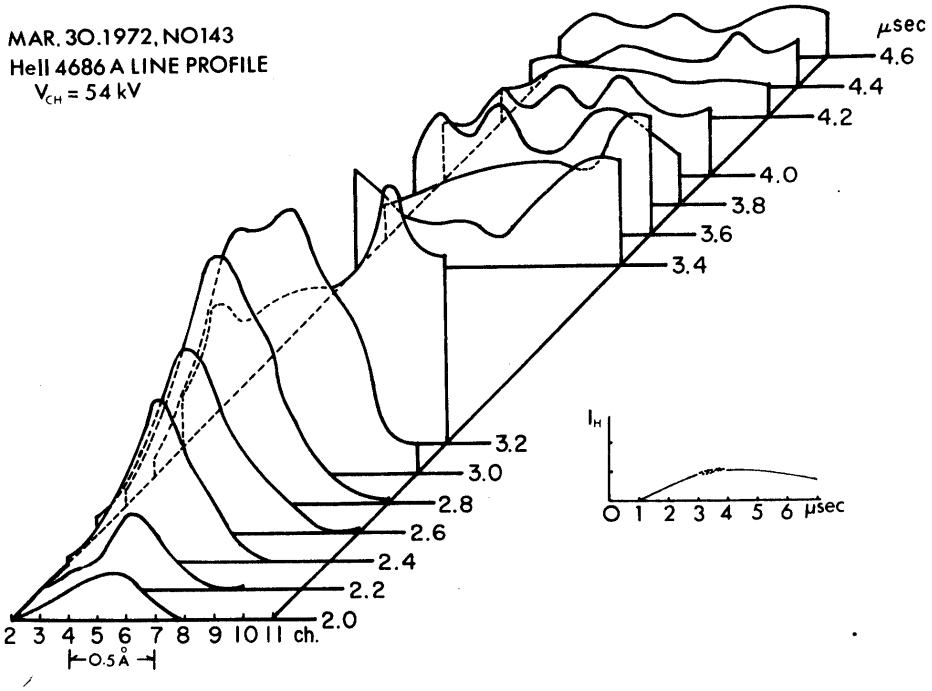
MAR. 30.1972, NO143
HeII 4686 A LINE PROFILE
V_{CH} = 54 kV
μsec
4.6
4.4
4.2
4.0
3.8
3.6
3.4
3.2
3.0
2.8
2.6
2.4
2.2
2.0
I_H
0 1 2 3 4 5 6 μsec
2 3 4 5 6 7 8 9 10 11 ch.
0.5 Å

Fig. 2

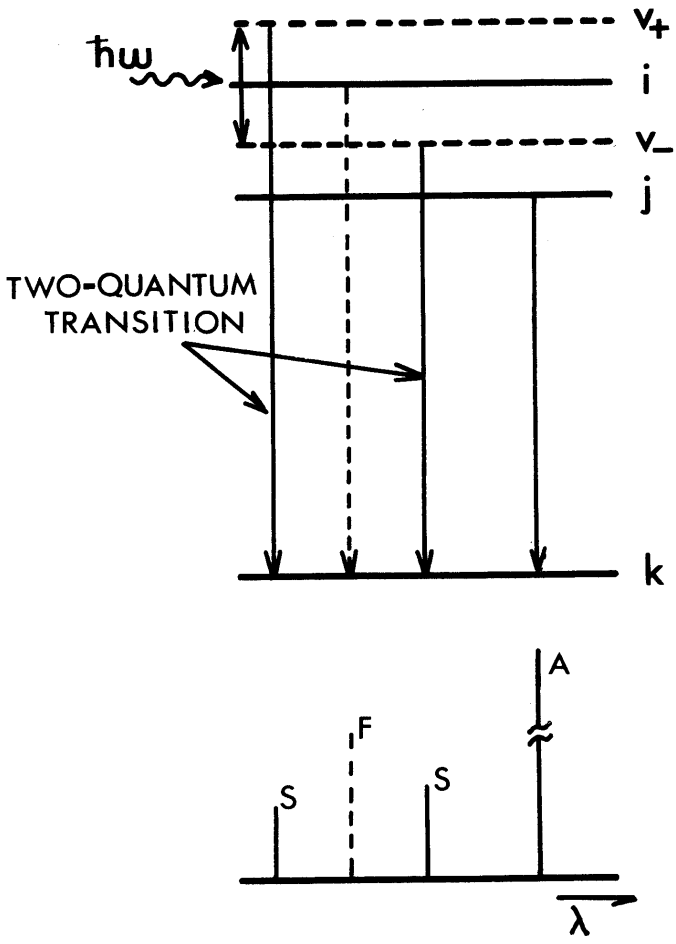

Fig. 3

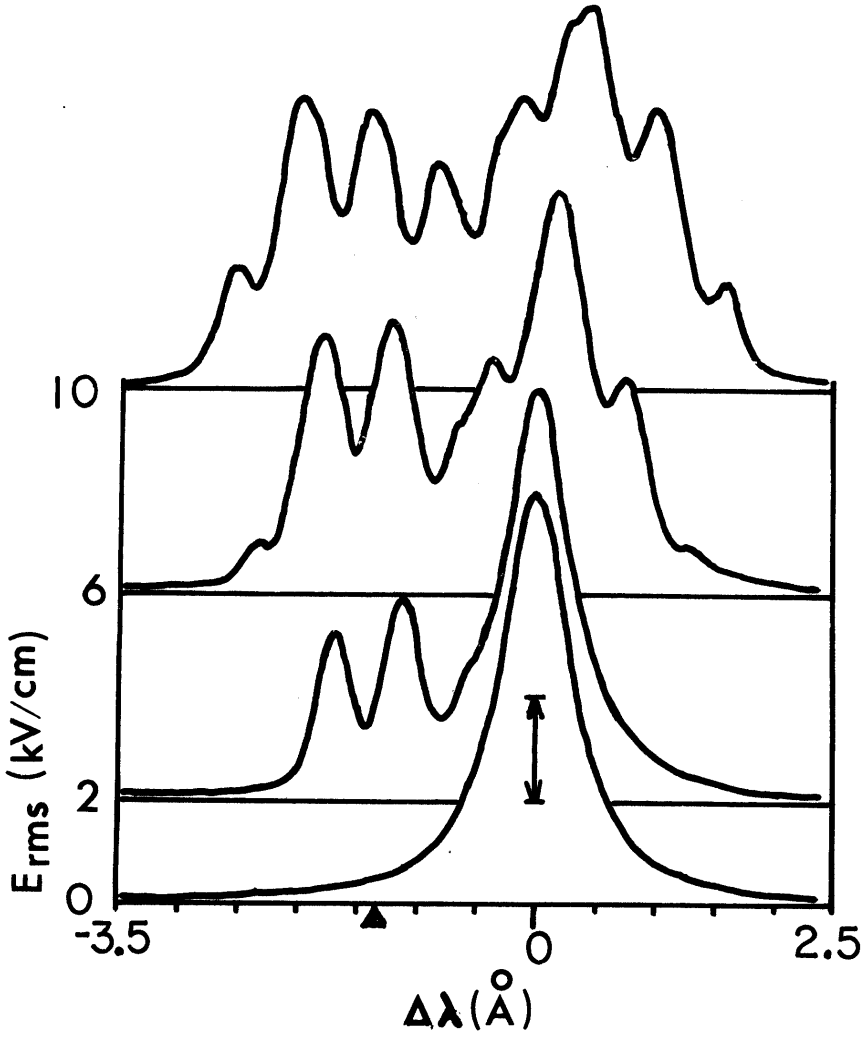

Fig. 4.

An Attempt to Determine Electron Temperature by the Measurement of Lyman Step of Helium Ion Continuum

S. Ohsumi and T. Ishimura

Faculty of Engineering, Osaka University, Osaka

In order to determine the electron temperature of high temperature plasmas, various methods are proposed and some of them are developed and put into practical use. In this paper, an experimental study to examine a method to determine the electron temperature is reported.

The principle of this method is summarized as follows. High temperature plasmas emit continuous spectrum which consists of free-free radiation (bremsstrahlung radiation) and free-bound radiation (recombination radiation). The spectral emissivity of the free-free radiation is a smooth function of wavelength λ, however, that of the free-bound one shows the discontinuous decrease at the wavelength λ_n of the n-th series limit. Therefore, the resultant spectral emissivity which is observed by experiment also shows the discontinuous decrease at the wavelength λ_n. The ratio R_n of the emissivity of the shorter wavelength side to that of the longer one is the known function of T_e/Z^2, where T_e is the electron temperature and Z is the atomic number of the ion. So, the electron temperature is determined by the measurement of the spectral emissivity of the both sides of the series limit.

Although the principle described above is well known, the actual application to the high temperature plasmas is not yet

done because of the technical difficulties. As is seen from Fig. 1[1], we are obliged to measure the ratio R_n at Lyman series limit (n = 1) in order to determine the electron temperature of the high temperature plasmas. The wavelength of Lyman series limit is 912 Å for hydrogen and 228 Å for ionized helium so that the spectroscopic measurement in the vacuum ultraviolet region is necessary.

In this experiment, a grazing incidence monochromator equipped with a concave grating of 1 m radius of curvature is used to measure the intensity of continuum of the both sides of Lyman series limit of ionized helium. In front of the incident slit of the monochromator, an aluminum foil of 0.1 μ thick is set to filter the light of which wavelength is shorter than about 150 Å so that the spectrum of higher order reflection does not overlap that of the first order one. This foil is also useful to reduce the noise originating in the stray light and to protect the grating and the detector against contamination by particles released from the plasma machine. Of course, a trap for the zero order reflection and baffles are equipped so as to eliminate the stray light. The detector is an open-window type photomultiplier with tungsten photocathode. Calibration of the relative spectral sensitivity of the whole measuring system is made by the branching ratio method[2] where a hollow cathode discharge tube is used as the light source. The results are shown in Fig. 2.

As the preliminary experiment, a helium plasma produced by a theta pinch gun is chosen as the subject of the spectroscopic measurement. The typical oscilloscope traces are reproduced in Fig. 3. From the ratio of the peak intensities, the electron temperature of the plasma is estimated to be (23 ± 5) eV in

this case.

Further, an theta pinch machine is constructed for the purpose to pursue this plan. The quartz discharge tube is 144 mm inner diameter and 500 mm long. The coil is 200 mm inner diameter and 310 mm long. The coil is excited by the discharge current of a condenser bank of 8 μF of which maximum charging voltage is 50 kV. The discharge current is crowbarred at the time of the current maximum. Besides, a preionization bank and a preheating bank are also provided.

Experiments are now going on and a few of the results are reported in this paper. In Fig. 4, the typical time sequences of the intensity of continuum of the both sides of Lyman series limit are shown in the case where the charging voltage of the main bank is 35 kV and the pressure of the helium gas is 50 mtorr. Observation is done through a port installed on the side of the discharge tube. The time origin is chosen to be the time of fire of the main bank. These figures are obtained by taking averages over the several oscilloscope traces so as to eliminate shot-to-shot fluctuations. In this case, the pinch time is about 1 μs, the diameter of the pinched plasma is about 5 cm and the time of the current maximum is 2 μs after the fire of the main bank. The time-resolved electron temperature is obtained from the ratio of the continuum intensity of the shorter wavelength side to that of the longer one and it is shown in Fig. 5.

Conclusively, it is proved experimentally that the time-resolved electron temperature is determined by the measurement of the continuum intensity of the both sides of Lyman series limit of ionized helium. In addition, it is shown that the theta pinch

machine is a useful light source for continuous spectrum in the vacuum ultraviolet region.

References

1) H. R. Griem: Plasma Spectroscopy (McGraw-Hill Book Co., New York, 1964).

2) E. Hinnov and F. W. Hofmann: J. Opt. Soc. Amer. 53, 1259 (1963).

Figure Captions

Fig. 1. Ratio R_n as the function of T_e/Z^2.

Fig. 2. Relative spectral sensitivity of the measuring system.

Fig. 3. Typical oscilloscope traces of continuum intensity from the helium plasma produced by the theta pinch gun, a) at 225 Å (shorter wavelength side), and b) at 250 Å (longer wavelength side).

Fig. 4. Typical time sequences (averages over several oscilloscope traces) of the continuum intensity from the helium plasma produced by the theta pinch machine, a) at 225 Å (shorter wavelength side), and b) at 239 Å (longer wavelength side).

Fig. 5. Temporal variation of the electron temperature of the plasma produced by the theta pinch machine.

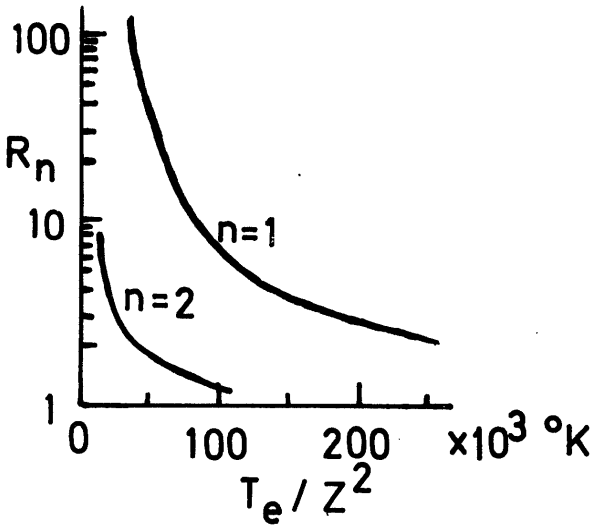

FIG. 1

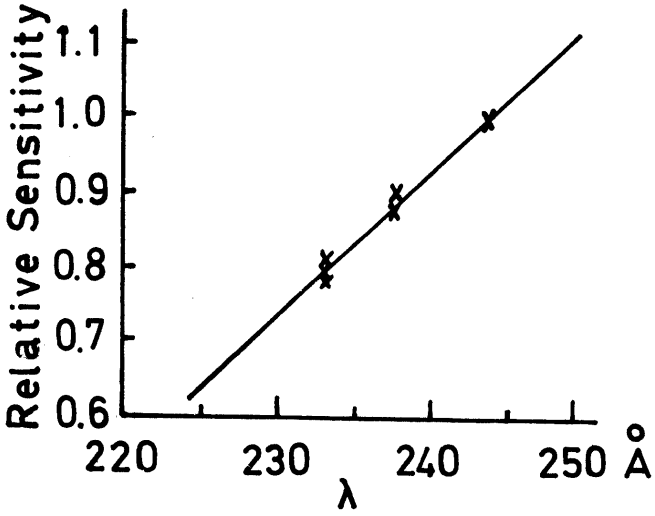

FIG. 2

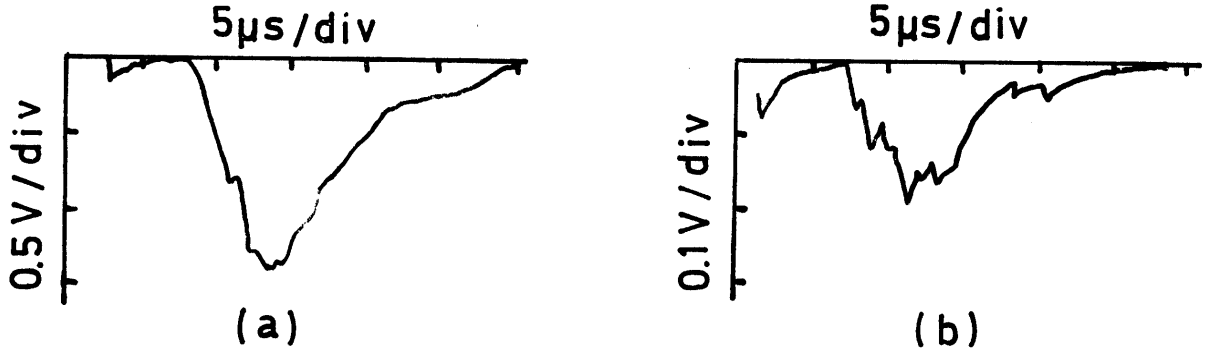

FIG. 3

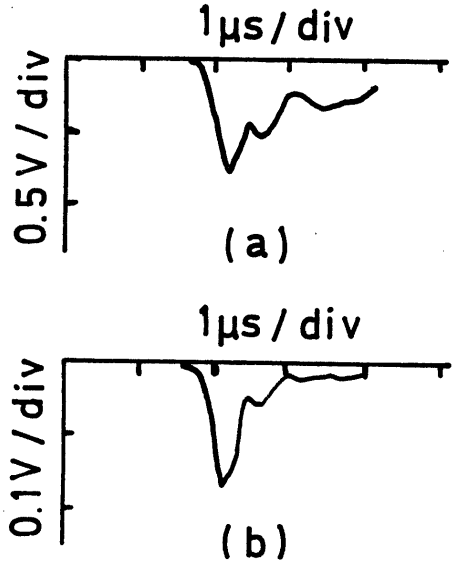

FIG. 4

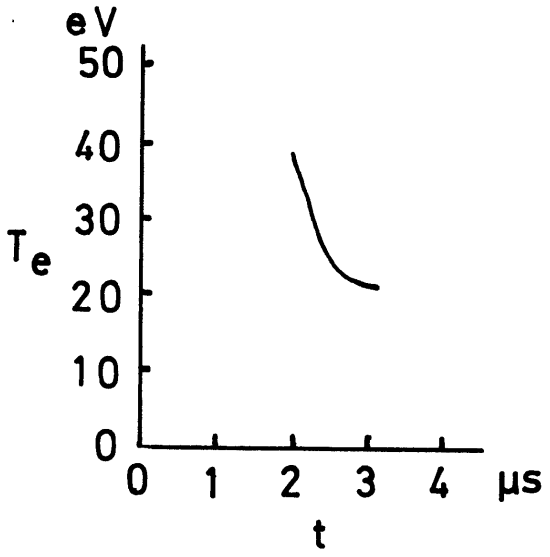

FIG. 5

Measurement of the Absolute Intensity of Radiation in the Soft X-Ray and Extreme Ultraviolet Region

H. Sugawara, T. Sasaki* and T. Oda**

Institute of Plasma Physics, Nagoya University, Nagoya

Establishing effective techniques for determination of the absolute intensity of radiation in the soft X-ray and extreme ultraviolet region of the spectrum (XUV) is required for plasma diagnostics, space research by means of rocket- or satellite-borne instruments, as well as solid state physics. The problem consists of two parts, one of which is to obtain the standard source of radiation and/or the standard detector, while the other is to establish the secondary standard which can be used conveniently in the practical application. Characteristics of various monochromators, gratings, detectors, and light sources will be in turn determined by using the secondary standard.

---

* Guest staff, present address: College of General Education, University of Tokyo, Komaba, Tokyo.

** Guest staff, present address: Department of Physics, Hiroshima Univeristy, Hiroshima.

The use of ionization chambers with rare gases has been proved appropriate as a primary standard detector in the region from 12 to 40 eV.[1] On the other hand the use of the synchrotron radiation as a standard source in XUV has been proposed.[2]

A heterochromatic calibration technique,[3] in which the both are combined, is described in this report. Then, a new method of the measurement of absolute intensity in XUV by means of energy analysis of photoelectrons is proposed.

Fig.1 shows the schematic drawing of the experimental arrangement for the heterochromatic calibration. The synchrotron radiation emitted by a 1.3 GeV electron syncrotron of the Institute for Nuclear Study, Tokyo, is introduced to the 0.5 m Seya type monochromator followed by a double ionization chamber. The end of the chamber may be terminated by a detector B or other devices which are to be calibrated. A part of the beam is interrupted by a mirror M in front of the entrance slit and led to a detector A which is not necessarily sensitive to XUV but may be of any conventional type, for instance, an ordinary photomultiplier for the use in visible or ultraviolet region of the spectrum. Two ion currents i_1 and i_2 of the ionization chamber are measured for determination of the photon flux I_o coming out of the monochromator by the following equation

$$I_o(\lambda) = \frac{i_1}{e^{-\mu L_1}(1 - e^{-\mu d})} \cdot \frac{1}{e\gamma} \qquad (1)$$

where e is the electronic charge, γ is the efficiency of photoionization, i.e., the number of emitted electrons per absorbed photon, L_1, L_2, and d are the geometrical constants of the apparatus, and μ is the absorption coefficient of the gas measured at a pressure P, and is given by the following equation

$$\mu(\lambda) = \frac{ln(i_1/i_2)}{L_2 - L_1} . \qquad (2)$$

If the rare gases are used, it is possible to select the region where γ equals unity.[1] The signal i_a from the monitoring detector A is recorded simultaneously with ion currents so that the effect of intensity fluctuation of the source is eliminated.

The more important advantage of this scheme is that the detector current i_a is heterochromatically "calibrated" at each λ by the simultaneous determination of $I_o(\lambda)$. As time dependence of i_a is the same as that of I_o, the fluctuation of the intensity is effectively cancelled out. Whereas the detector A accepts entirely different spectral range from the ion chamber and i_a is independent of the wavelength λ in which the photon flux is being measured, it keeps the memory of $I_o(\lambda)$ after the calibration. It is only possible for the light source like the synchrotron radiation in which the spectral distribution is fixed and independent of the intensity as far as the maximum energy of electrons and the mode of operation remain unchanged.

Some examples of application are shown in Fig.2, 3 and

4. Figure 2 shows the spectrum of the absolute intensity of the radiation obtained through a system of an aluminum coated concave prereflector at 75° incidence and a 50 cm Seya-type monochromator equipped with a gold coated Bausch and Lomb grating of 1200 lines per mm.[4] The operational energy of the synchrotron is 700 MeV. The ordinate is the ratio of the absolute intensity to the simultaneous signal of the secondary standard. Rare gases used in the ionization chamber were He in the wavelength region 300 to 504 Å, Ar 300 to 786 Å (dotted curve up to 450 Å), and Xe 500 to 1000 Å (dotted curve up to 700 Å). The deviation of the dotted curve from the full curve shows the existence of secondary process, namely the ionization of neutral atoms due to energetic photoelectrons in the ionization chamber. The application of the ionization chamber to higher photon energy region is limited by the existence of the secondary process. Figure 3 shows the spectral efficiency of the system of the prereflector and the monochromator.[5] Since determination of the number of electrons circulating in the synchrotron orbit was made only approximately, the values indicated are not claimed very exact. Figure 4 shows the relative spectral sensitivities of two EMI open photomultipliers 9603-1 with AgMg dynodes and 9603-2 with BeCu dynodes.[5]

There are some problems in this techniques to be mentioned. Since the synchrotron radiation is the perfect continuum without any overlapped line spectra, the higher order diffraction of the grating and the stray light should be treated more carefully than usual. Determination of

$I_o(\lambda)$ with more than two kinds of gases of different ionization potentials in a same region of wavelength is often helpful in estimating these spurious components. In the present measurements the results above 30 eV are less reliable than the other part.

A new method[6] for the measurement of absolute intensity in XUV by means of energy analysis of photoelectrons emitted from rare gas atoms is proposed, which is also applicable to higher photon energy region. If a gas is irradiated by monochromatic radiation (photon energy $\hbar\omega$), there will result many groups of photoelectrons. The energy ε_ν of the photoelectrons of each group is given by

$$\varepsilon_\nu = \hbar\omega - E_I - E_\nu \ , \qquad (3)$$

where E_I is the ionization potential of the atom and E_ν is the excitation potential of the level ν of the ion with respect to the ground state. The energy level scheme of helium ion is the simplest of all the rare gases as it is hydrogen-like and consequently it is most suitable for the present purpose, and its lowest value E_2 is 40.8 eV.

Any type of electron energy analyzer may be used for the present purpose, but two factors should be considered in order to obtain the better results. Firstly the efficiency of the analyzer in collecting electrons should be easily determined or evaluated. Secondly, it should be so designed as to collect as many electrons as possible,

because the overall sensitivity of the detector will be low.

Figure 5 shows the block diagram of the experimental arrangement. The apparatus consists of two parts; an electron energy analyzer of spherical retarding field type and a system of the detection of the photoelectron signal. Monochromatic radiation of photon energy $\hbar\omega$ and intensity I_o is introduced to the interacting region of length ℓ, including the center of the four concentric grids. The analyzer is filled with target gas at a density N cm^{-3}. Part of the photoelectrons produced within the interacting region will be analyzed by the retarding potential between the first and second grids, and then accelerated and focused on a channel electron multiplier. The signals from the channel electron multiplier are amplified, discriminated, counted and recorded in number. The retarding potential fed to the analyzer is controlled by a flag signal from the digital recorder.

More of the photoelectrons will be lost through collisions with the gas mainly in the analyzing region, and this loss should be approximately $N\,\sigma_e\,r$, where σ_e is the total cross section of scattering for electrons and r is the radius of the analyzing sphere. It will be negligibly small at pressures as low as 10^{-4} torr. The differential count $n(\varepsilon_1, \omega)$ of collected electrons for $eV_R = \varepsilon_1$ against the monochromatic radiation of photon energy which satisfies eq.(3) should be thus

$$n(\varepsilon_1, \omega) = I_o(\omega) N \sigma_1(\omega)\ \ell\ \eta (1 - N\,\sigma_e\,r) \qquad (4)$$

where $\sigma_1(\omega)$ is the photoionization cross section for the ground state ion, and η is the efficiency of collecting photoelectrons which is dependent upon the overall transparency of grids, the angular aperture of the analyzer, the angular distribution of photoelectrons, and the polarization of incident radiation. This quantity is determined by calibration with an ionization chamber at an appropriate wavelength.

A tentative evaluation of this value at $\hbar\omega$ = 66.6 eV for helium where data is available[7] gives a typical count of order of 10^2 S^{-1} for 10^8 incident photons per sec. The preliminary experiment, which was made under the similar condition, showed $n(\varepsilon_1, \omega) \sim 160$ counts/sec. It should be noted that the wavelength of radiation being detected is simultaneously determined in this method by the energy analysis of photoelectrons and therefore one may omit the monochromator from the system.

References

1) J. A. R. Samson: J. Opt. Soc. Amer. 54 (1964) 6.

2) T. Oshio, M. Sasanuma and T. Sasaki: Buturi (in Japanese) 22 (1967) 285.

3) T. Sasaki: Proc. Intern. Symp. for Synchrotron Radiation Users, Daresburg Nuclear Physics Laboratory, January 1973, p.142.

4) T. Sasaki and H. Sugawara: Ann. Rev. of Inst. Plasma Phys. Nagoya Univ., Apr. 1971 - Mar. 1972, p.119.

5) T. Sasaki and H. Sugawara: Ann. Rev. of Inst. Plasma Phys. Nagoya Univ., Apr. 1970 - Mar. 1971, p.115.

6) T. Sasaki, T. Oda and H. Sugawara: Ann. Rev. of Inst. Plasma Phys. Nagoya Univ., Apr. 1971 - Mar. 1972, p.118; Proc. Intern. Symp. for Synchrotron Radiation Users, Daresburg Nuclear Physics Laboratory, January, 1973, p.145.

7) J. A. R. Samson, Phys. Rev. Letts. 22 (1969) 693.

Figure Captions

Fig.1. Schematic drawing of the experimental arrangement for the heterochromatic calibration.

Fig.2. Spectral absolute intensity of the radiation coming from the monochromator. The dotted curves show the existence of secondary process in the ionization chamber.

Fig.3. Spectral efficiency of a system of an aluminum-coated concave prereflector at 75° incidence and a gold-coated Bausch & Lomb grating (radius: 0.5 m, rulings: 1200 lines/mm, blaze: 700 Å).

Fig.4. Spectral sensitivities of two EMI-multipliers. A: 9603-1, with AgMg dynodes and cathode. B: 9603-2, with BeCu dynodes and cathode.

Fig.5. Block diagram of the experimental arrangement for measuring the absolute intensity of XUV radiation by photoelectron spectroscopy.

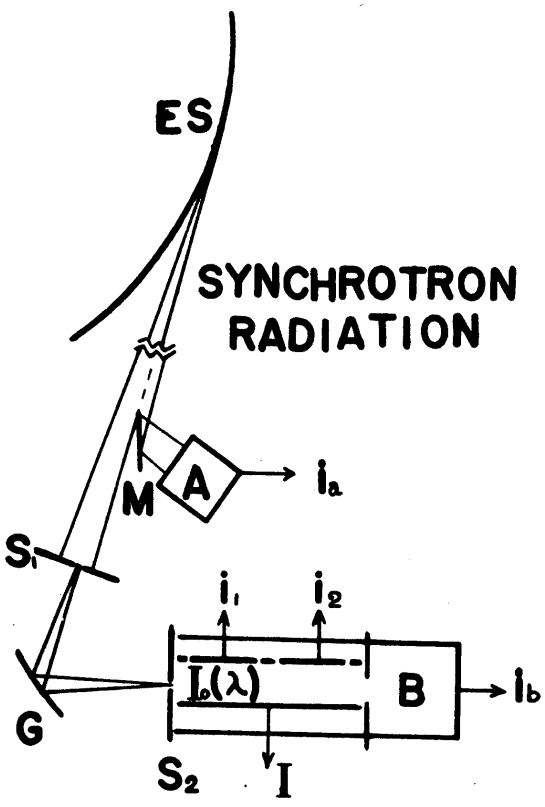

Fig. 1

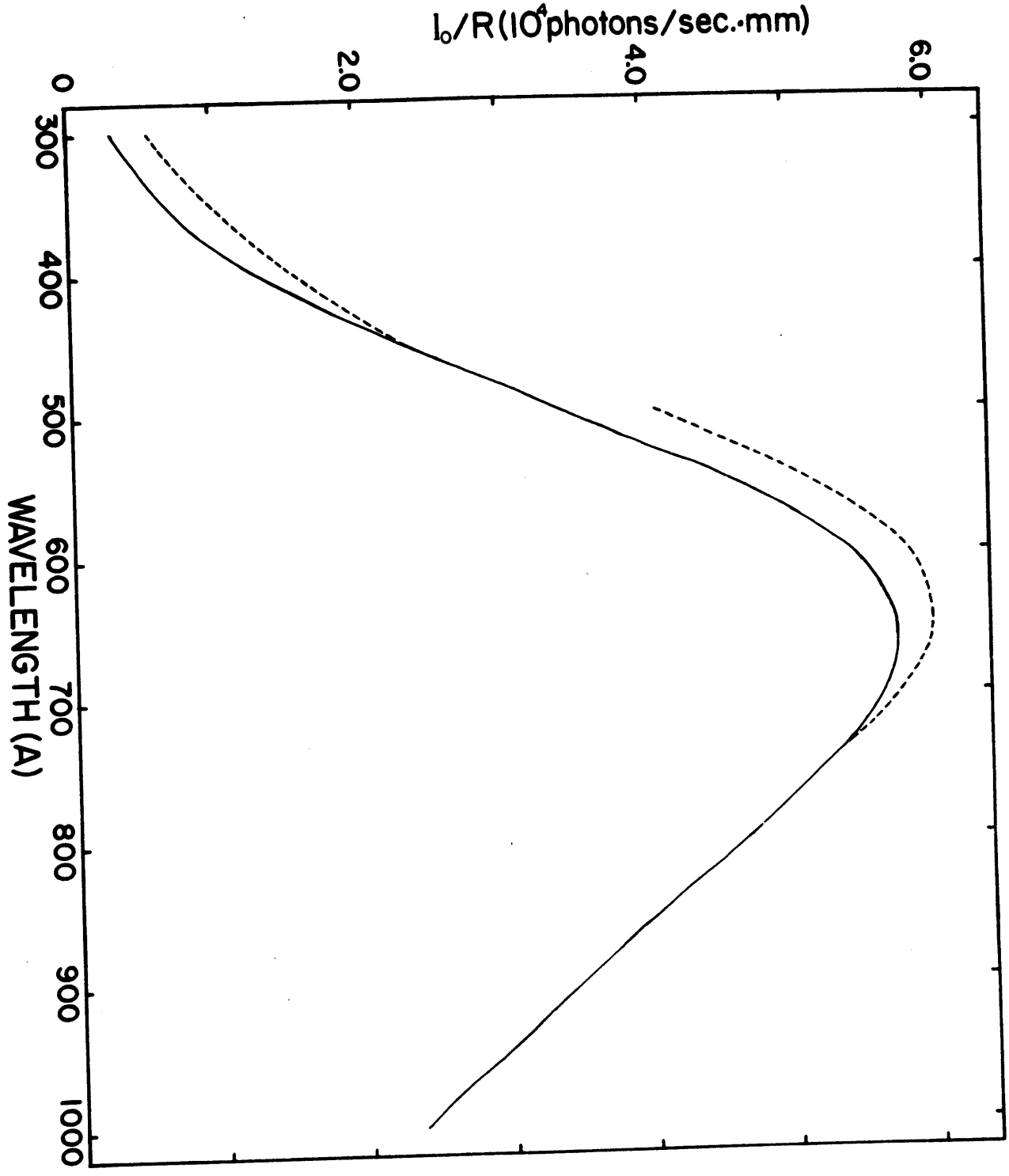
$I_o/R(10^4$photons/sec.-mm)
0
2.0
4.0
6.0
300
400
500
600
700
800
900
1000
WAVELENGTH (A)

Fig. 2

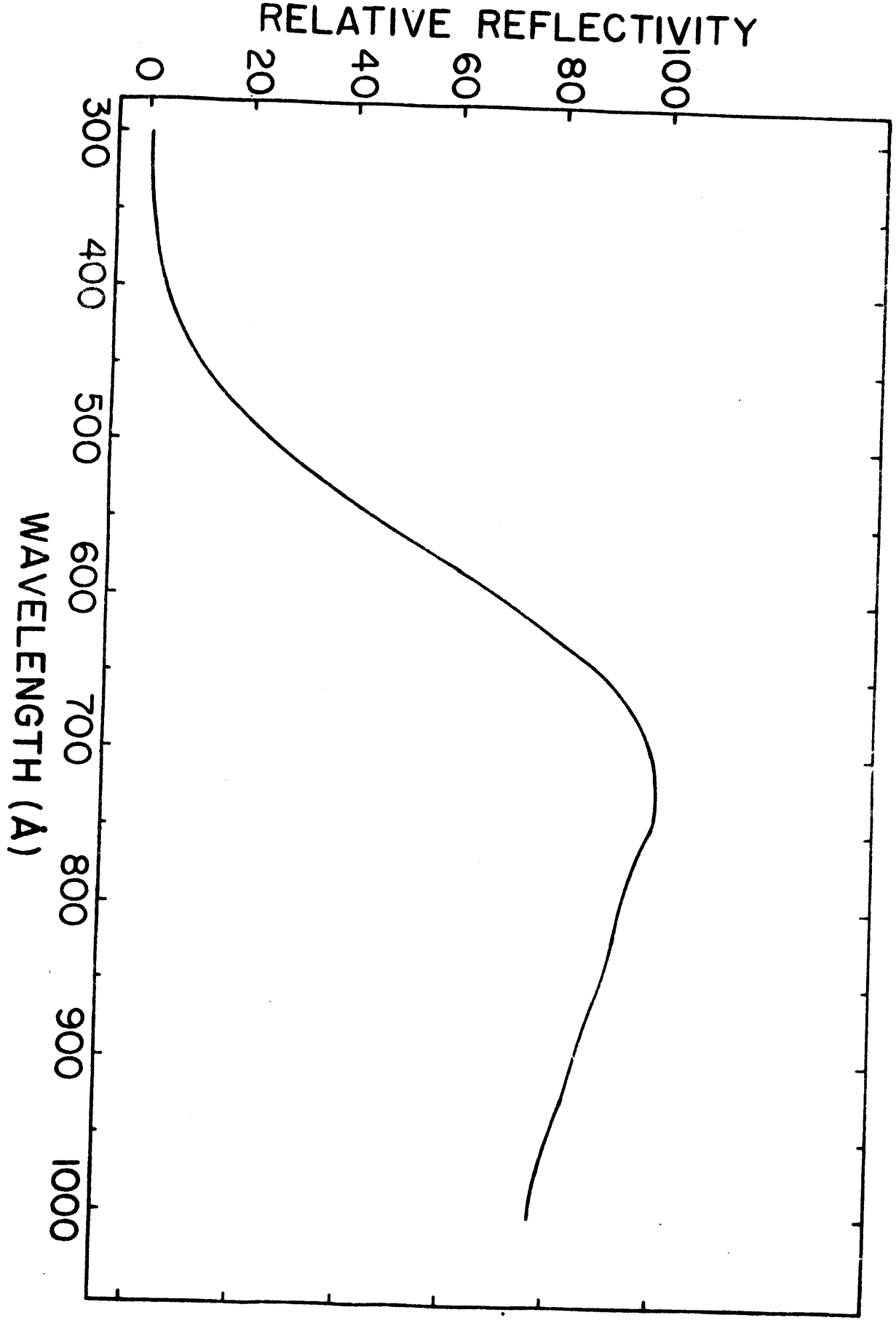
RELATIVE REFLECTIVITY
0
20
40
60
80
100
WAVELENGTH (Å)
300
400
500
600
700
800
900
1000

Fig. 3

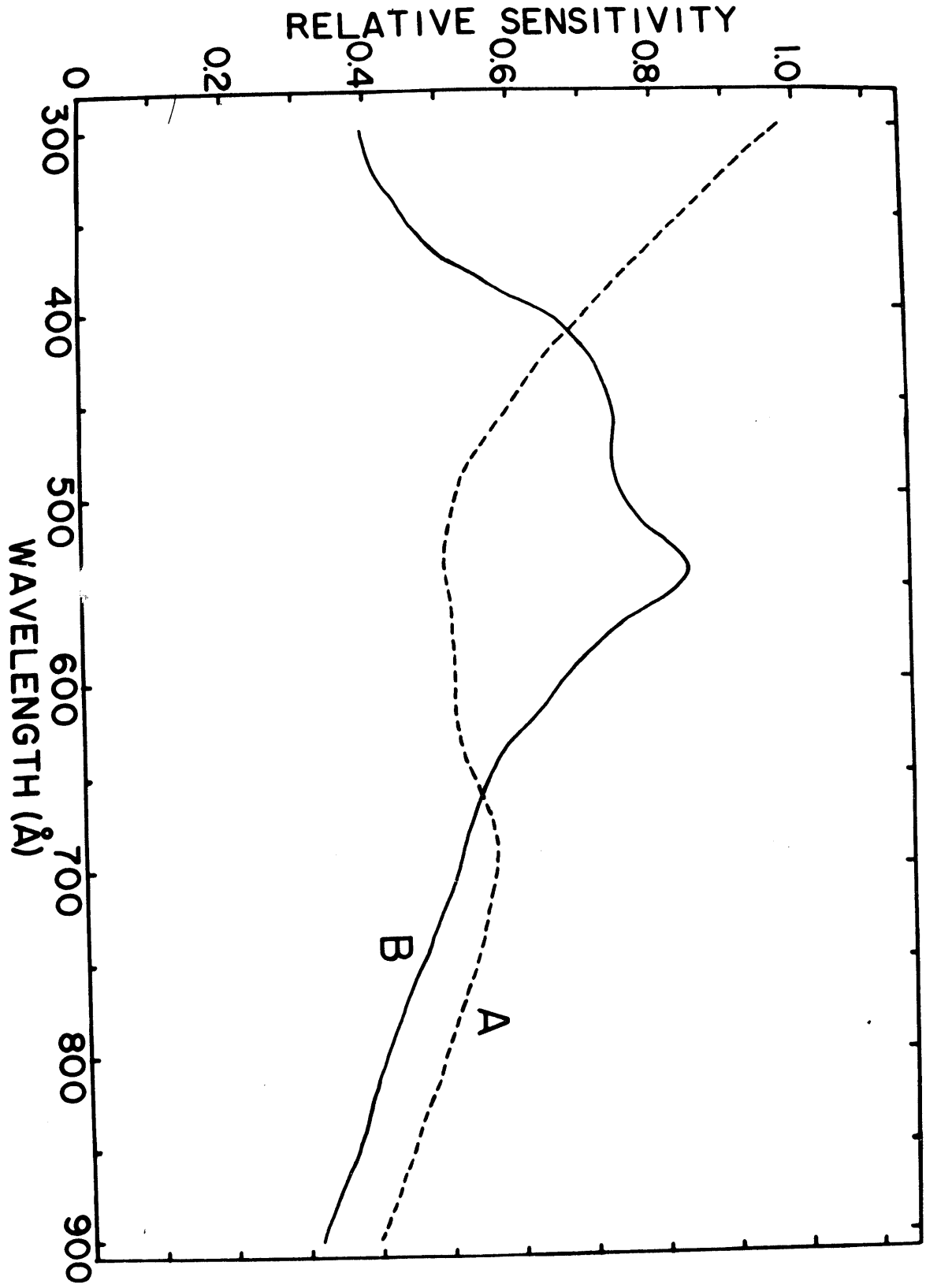
RELATIVE SENSITIVITY
0
0.2
0.4
0.6
0.8
1.0
WAVELENGTH (Å)
300
400
500
600
700
800
900
B
A

Fig. 4

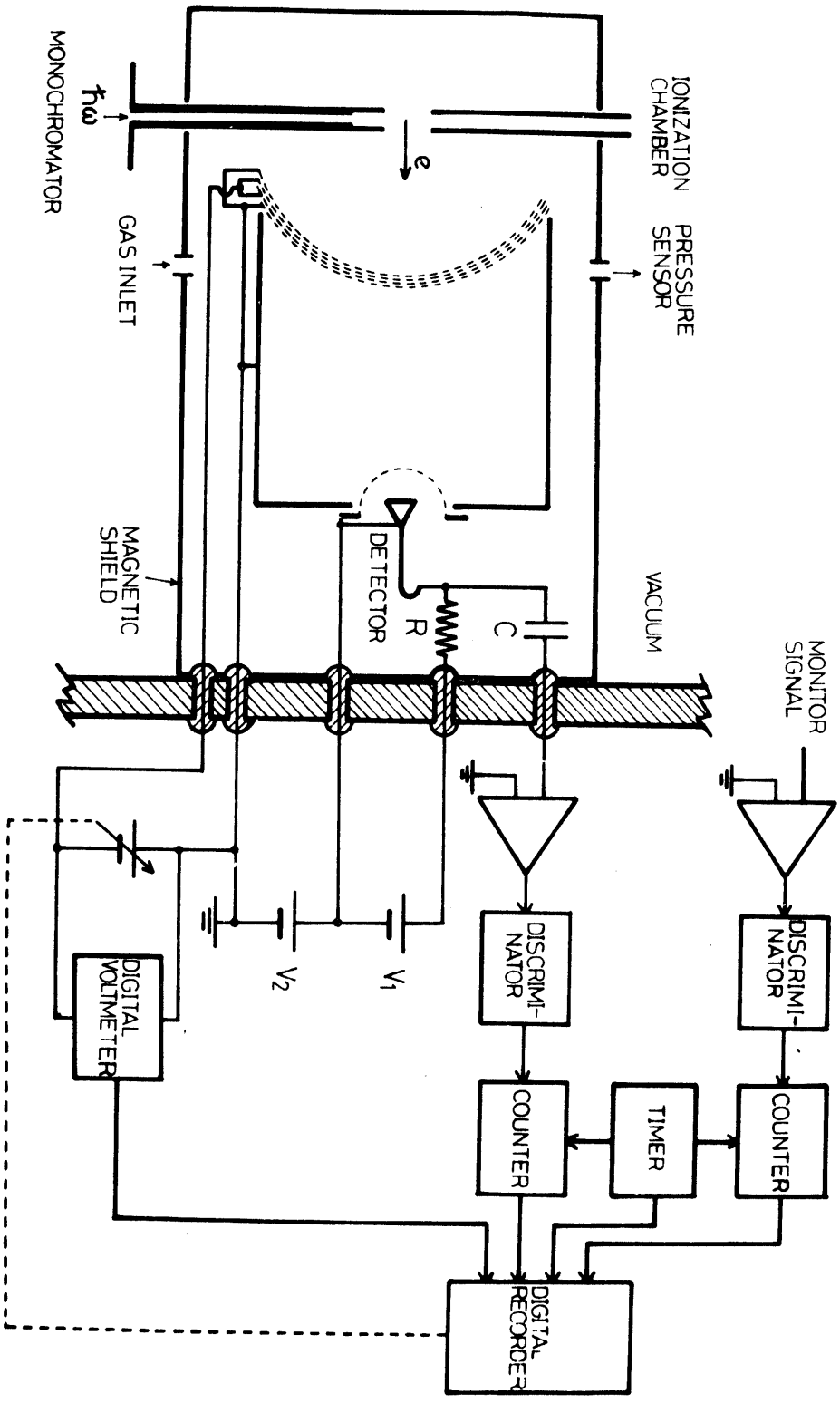
MONOCHROMATOR
ħω
GAS INLET
IONIZATION CHAMBER
e
PRESSURE SENSOR
MAGNETIC SHIELD
DETECTOR
R
C
VACUUM
MONITOR SIGNAL
DIGITAL VOLTMETER
V2
V1
DISCRIMI-NATOR
DISCRIMI-NATOR
COUNTER
TIMER
COUNTER
DIGITAL RECORDER

Fig. 5

Laser light scattering from a turbulently heated plasma

K. Kondo

Institute of Plasma Physics, Nagoya University
Nagoya, Japan

Turbulent heating of a plasma is one of the most effective method for heating a plasma. There have been many experiments and theories about turbulent heating. Though we have been accumulated many experimental results understanding the heating mechanism using diamagnetic effect and X-ray radiation etc., spatially inhomogenity and rapid temporal variation of the plasma parameters lead one in confusion to identify instabilities which result plasma heating. For such a non-ideal plasma, laser scattering is a promising diagnostic technique to obtain the informations about the electron velocity distribution with high spatial and temporal resolution.

Usually giant pulse Rb-laser (6943 Å) is used for light scattering. We can determine the electron velocity distribution from the spectrum of scattered light broadening by the Doppler effect, on condition that scattering parameter $\alpha = \lambda/(4\pi\lambda_D \sin\theta/2)$ is less than 1; λ=6943Å; λ_D: electron Debye length; θ: scattering angle. In contrast with this, when α is larger than 1 (forward scattering), large scale density fluctuation reveals in the spectrum. Though it is very interested in obtaining the spectrum of small angle scattering from a turbulent plasma, to perform such a measurement for a low density and high temperature plasma is actually very difficult.

We limit ourselves to only 90° light scattering i.e. $\alpha \ll 1$. Relation of the intensities between incident laser beam, I_0, and scattered, $I(\lambda_0)$, is expressed as follows;

$$I(\lambda_0) = a I_0 n_e V \sigma_T \, d\Omega \int_{\lambda_0 - \frac{\Delta\lambda}{2}}^{\lambda_0 + \frac{\Delta\lambda}{2}} S(\lambda) g(\lambda - \lambda_0) d\lambda$$

a; loss due to the optical system

n_e; electron density

V; scattering volume

σ_T; Thomson cross section

$d\Omega$; solid angle gathering the scattered light

$S(\lambda)$; spectrum of scattered light

$g(\lambda-\lambda_0)$; slit function centered at wave length λ_0

$\Delta\lambda$; slit width measured in wave-length

If both $S(\lambda)$ and $g(\lambda-\lambda_0)$ are Gaussian, $I(\lambda_0)$ is also Gaussian, and there is a relation among every half width as follows;

$$\Delta^2_{I(\lambda_0)} = \Delta^2_{S(\lambda)} + \Delta^2_{g(\lambda-\lambda_0)},$$

and the electron temperature T_e is determined from the formula,

$$\Delta_{S(\lambda)}(\mathring{A}) = 32.3\sqrt{T_e(eV)} .$$

The electron density is proportional to the integration of $S(\lambda)$ with total wave length. There are two methods to obtain the electron density, the first is to count absolute photon number scattered from plasma electrons, the other to calibrate the whole optical system by means of Rayleigh scattering from a neutral gas. Usually nitrogen is used for Rayleigh scattering, and scattered intensity $I(\lambda_0)_{N_2}$ is,

$$I(\lambda_0)_{N_2} = a I_0 n_{N_2} V \sigma_R \, d\Omega \int_{\lambda_0-\frac{\Delta\lambda}{2}}^{\lambda_0+\frac{\Delta\lambda}{2}} S_N(\lambda) g(\lambda-\lambda_0) d\lambda$$

Using above formula and one for plasma electrons, we obtain

$$n_e = n_{N_2} \frac{I(\lambda_0)\, \sigma_R \int S_N(\lambda) g(\lambda-\lambda_0) d\lambda}{I(\lambda_0)_{N_2} \sigma_T \int S(\lambda) g(\lambda-\lambda_0)\, d\lambda}$$

n_{N_2} is given by reading the N_2-pressure, and we use the experimental value for $I(\lambda_0)$ and $I(\lambda_0)_{N_2}$.

We can check the lower limit of the electron density to be measured by laser light scattering by means of Rayleigh calibration. In actual optical system, it is inevitable to remove stray light, mainly due to wall reflection, and this stray light gives the lowest electron density to be measured.

Fig.1. shows one case of the relation between the stray light and Rayleigh scattered light. 0.3 Torr N_2-pressure is a critical value below which Rayleigh scattered light is masked by the stray light. Considering the ratio of the cross section σ_R/σ_T, this value corresponds to 3×10^{13} cm^{-3} electron density. However the electron temperature is high enough, we can measure lower density plasma than the above value though we can not know the spectrum near 6943 Å, because Doppler broadening due to the themal electron is larger than the stray light. The latter is determined by the slit width of the detector.

If $I(\lambda_0)$ is not Gaussian, we can only discuss about the electron velocity distribution averaged over the slit width.

Fig.2. is one of the examples of the spectrum before and during the turbulently-heating process. Measurements are done at the 2 cm off from the axis of the plasma column, where the heating current flows and seems to excite some instabilities at 1 μsec after the initiation of the turbulent heating.

We have difinite difference in the spectrum profile between the initial and the heated plasma. The velocity

distribution of the initial plasma is Maxwellian, but for the heated one we can not say to be Maxwellian.

Now we have been continued to investigate what mechanisms change the electron velocity distribution.

Figure Captions

Fig.1. Rayleigh calibration of the optical system.

Fig.2. Spectrum profiles of the scattered light from the initial and heated plasma.

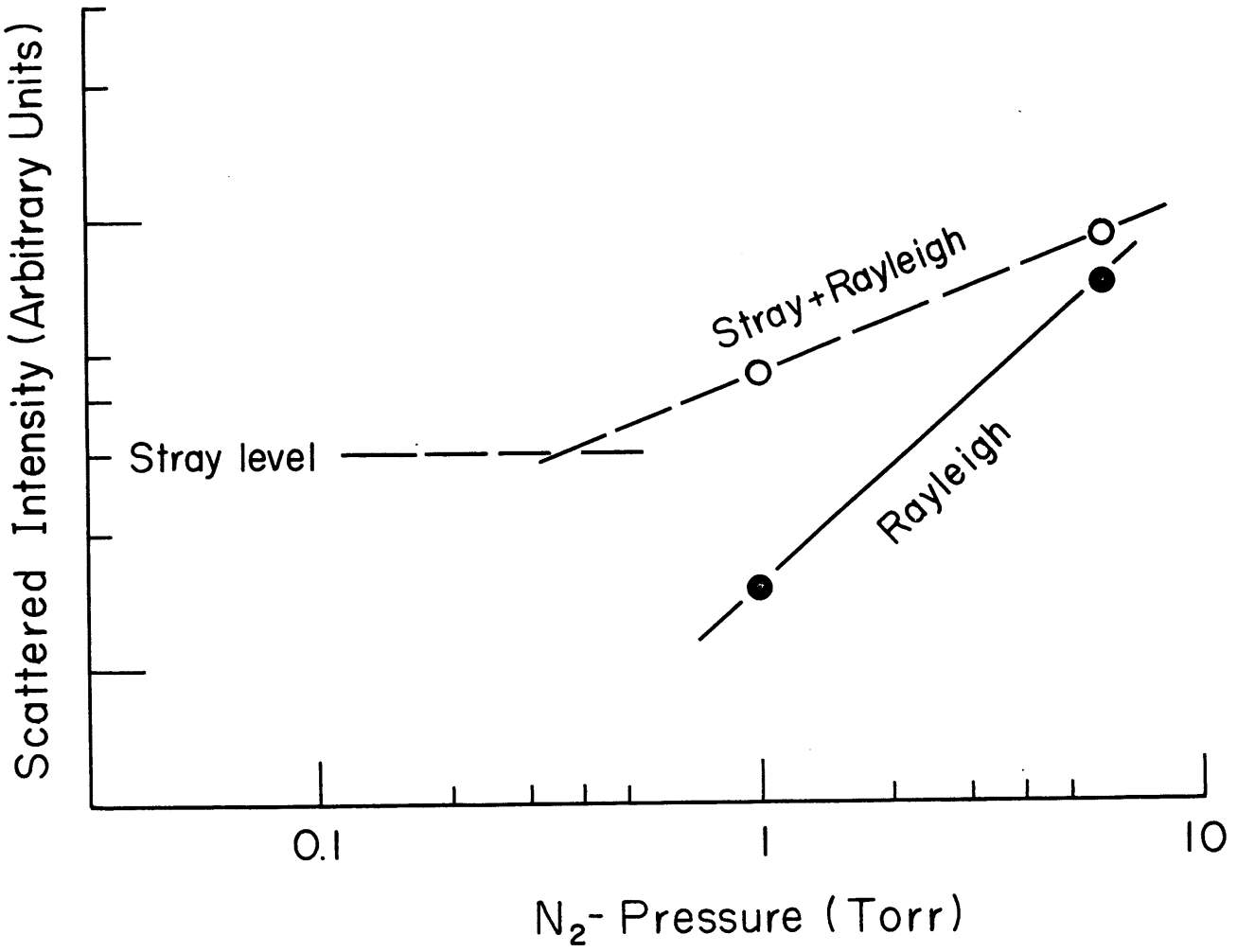
Scattered Intensity (Arbitrary Units)
Stray+Rayleigh
Stray level
Rayleigh
0.1
1
10
N2- Pressure (Torr)

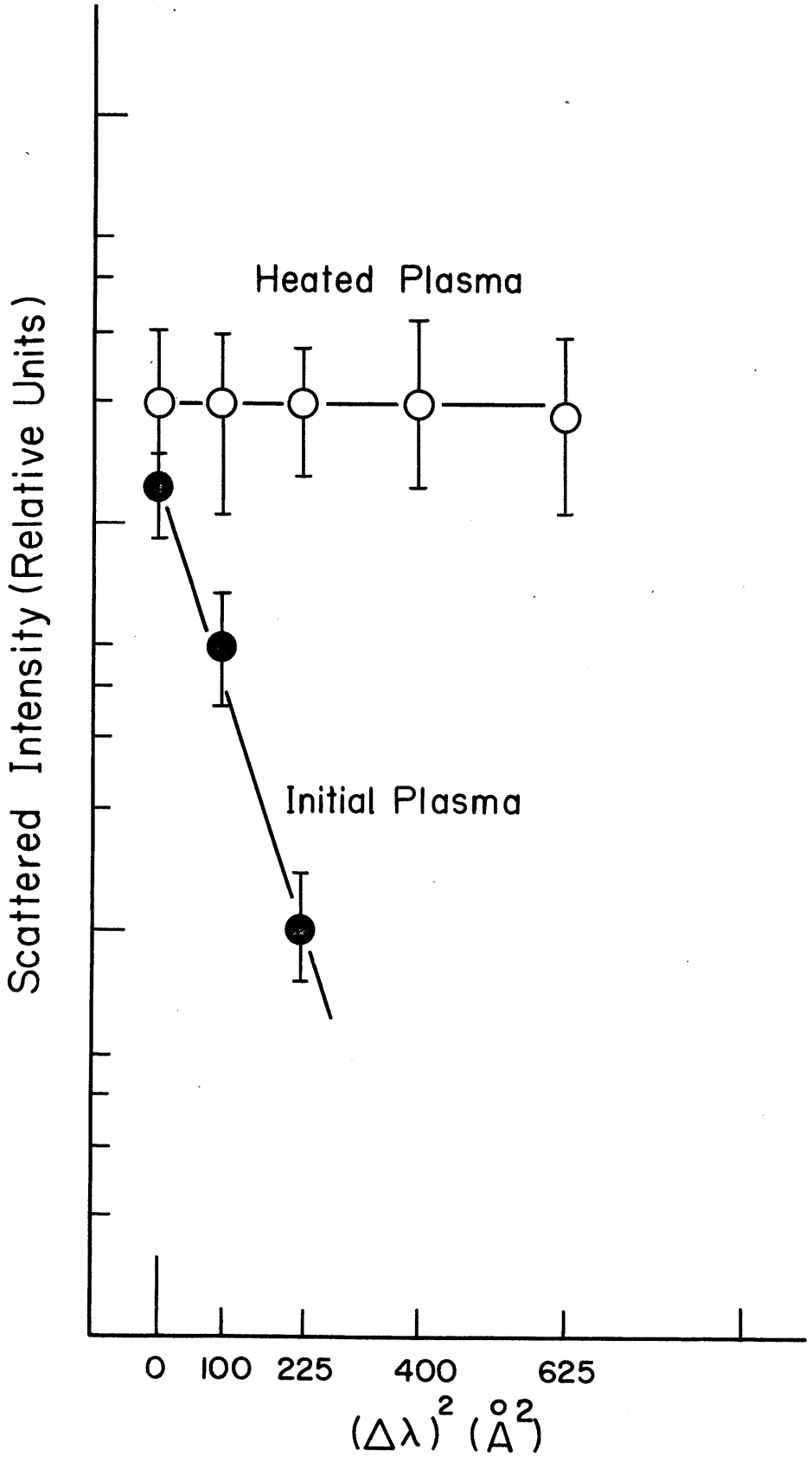
Heated Plasma
Initial Plasma
Scattered Intensity (Relative Units)
0
100
225
400
625
$(\Delta\lambda)^2$ ($\mathring{A}^2$)

Relativistic Corrections to the Spectrum of Scattered Light from a High Temperature Plasma

Kiyoshi Hayase and Takayoshi Okuda
Department of Electronics, Faculty of Engineering,
Nagoya University

The laser scattering is one of powerful diagnostic techniques in high temperature plasmas. It provides local values of electron temperature and density and even turbulence without perturbing the plasma.[1] The theory of light scattering used in the experiment was developed for the cold electrons. There was no consideration for the relativistic behaviors of electrons. The electron temperature of plasmas for which the laser scattering has been applied ever since, typically in a theta-pinch and Tokamak, is as high as a few keV.[2] It seems to require the relativistic corrections to the conventional theory. The relativistic effect was observed in a high energy electron beam and the comparison with the theoretical prediction was made.[3] The relativistic correction for a thermal plasma can be calculated taking into account a relativistic Maxwellian distribution of electron velocity. It is expected that the tail of Gaussian profile of the spectrum of the scattered light is modified. This modification of profile must be considered when we estimate the electron temperature from the spectral broadening of the scattered light. We will consider the modification of the scattering crossection in a high energy region and its

effect on the temperature estimation.

The electromagnetic wave scattered by a single electron $\vec{E}_s(R,t)$ which is irradiated by an incident plane electromagnetic wave $\vec{E}_i(t)$ is expressed as

$$\vec{E}_s(R,t)=\frac{e^2}{mc^2}(1-\beta^2)^{1/2}\frac{\vec{s}\times\{(\vec{s}-\vec{\beta})\times\vec{E}_i+\vec{\beta}\times(\vec{i}\times\vec{E}_i)-\vec{\beta}(\vec{\beta}\cdot\vec{E}_i)\}}{R(1-\vec{s}\cdot\vec{\beta})^3}$$

$$\times\cos(k_sR-\omega t-\vec{k}_i\cdot\vec{r}(0)) \qquad 1$$

where $\vec{s}$ is the unit vector directing the observing point, $\vec{i}$ the unit vector along the propagation of incident wave, k_s and ω_s the wave vector and angular frequency of the scattered wave, respectively, $\vec{\beta}$ the velocity of electron normalized by c and others as usual.

When the incident wave polarized in the z direction propagates in the x direction and the scattered wave is observed in the y direction in a Cartesian coordinate system, the power of the scattered wave is calculated easily for the unidirectional monochromatic electron beam. The scattering crossection for the electron with velocity v_x in the x direction σ_x is calculated to be

$$\frac{\sigma_x}{\sigma_c}=(1-\beta_x^2)(1-\beta_x)$$

where σ_c is the scattering crossection for the nonrelativistic electron. Similarly, the scattering crossections are calculated for the beams with v_y and v_z.

$$\frac{\sigma_y}{\sigma_c}=(1+\beta_y)/(1-\beta_y)^3$$

$$\frac{\sigma_z}{\sigma_o} = (1-\beta_z^2)^3$$

In the above calculation, the scattered wave with the z polarization is considered only. These results are shown in Fig.1. As seen from the figure, the crossection increases abruptly with β_y in the direction of observation , while it decreases with β_x and β_z. The relativistic correction seems necessary at β larger than 0.1.

As the velocities of electrons are distributed in a thermal plasma, the spectrum of the scattered light is broadened with the following relations.

$$\vec{k}_s = \vec{k}_i + \vec{k}$$

$$\omega_s = \omega + \Delta\omega$$

where $\vec{k}$ is the scattering vector and $\Delta\omega$ the frequency shift of the scattered wave.

When the velocities of electrons are distributed isotropically and the distribution function is Maxwellian, the profile of the spectrum of the scattered light is Gaussian in a nonrelativistic approximation at α much smaller than unity. The scattering intensity is increased or decreased in the tails of the profile in the blue or red sides, respectively as is expected from the calculation of the scattering crossections.

The examples of the profiles for 100 and 500 eV are shown in Fig.2, considering only the zero and first order terms of β, where the finite transit time effect is taken

into account.[4] The correction is not necessary in practice at 100 eV. However, it is appreciable at the temperature higher than 500 eV. If we take the half width for the estimation of the electron temperature, we get 441 eV in the red side and 560 eV in the blue side. Then, we overestimate and underestimate the values as much as about 10 in the blue and red sides, respectively. The second or higher terms of ß must be considered for the higher temperature. The calculations are being continued for the electron temperature higher than 1 keV and will be reported elsewhere.

References

1) D.E.Evans and J.Katsenstein Rep.Prog.Phys. 32 (1969) 207

2) M.J.Forrest et al. CLM-R 107 (1970)

3) G.Ward, R.E.Pechacek and A.W.Trivelpiece Phys.Rev. 3 (1971) 1721

4) R.E.Pechacek and A.W.Trivelpiece Phys.Fluids 10 (1967) 1688

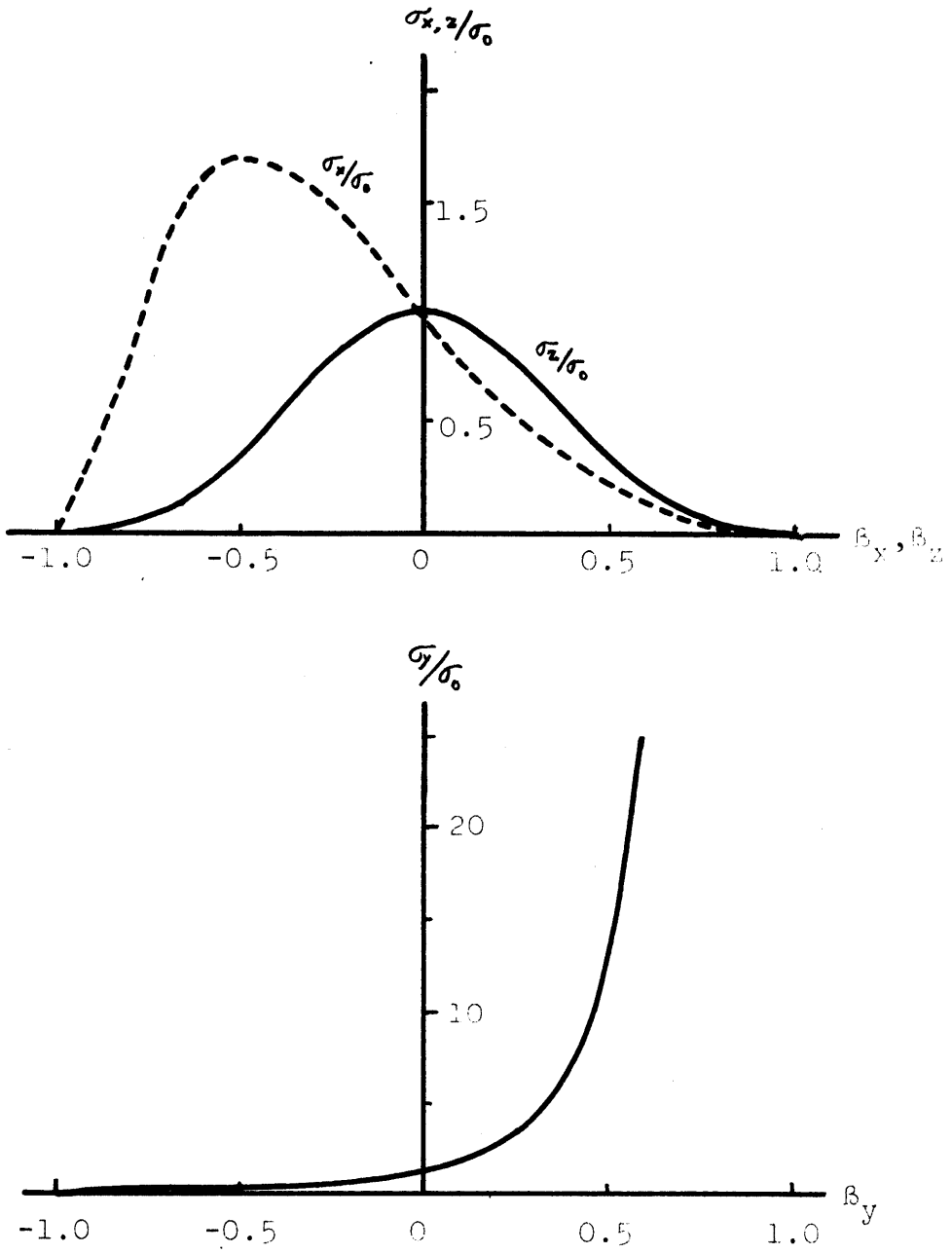

Fig.1. Dependence of relative scattering crossections on β_x, β_y and β_z.

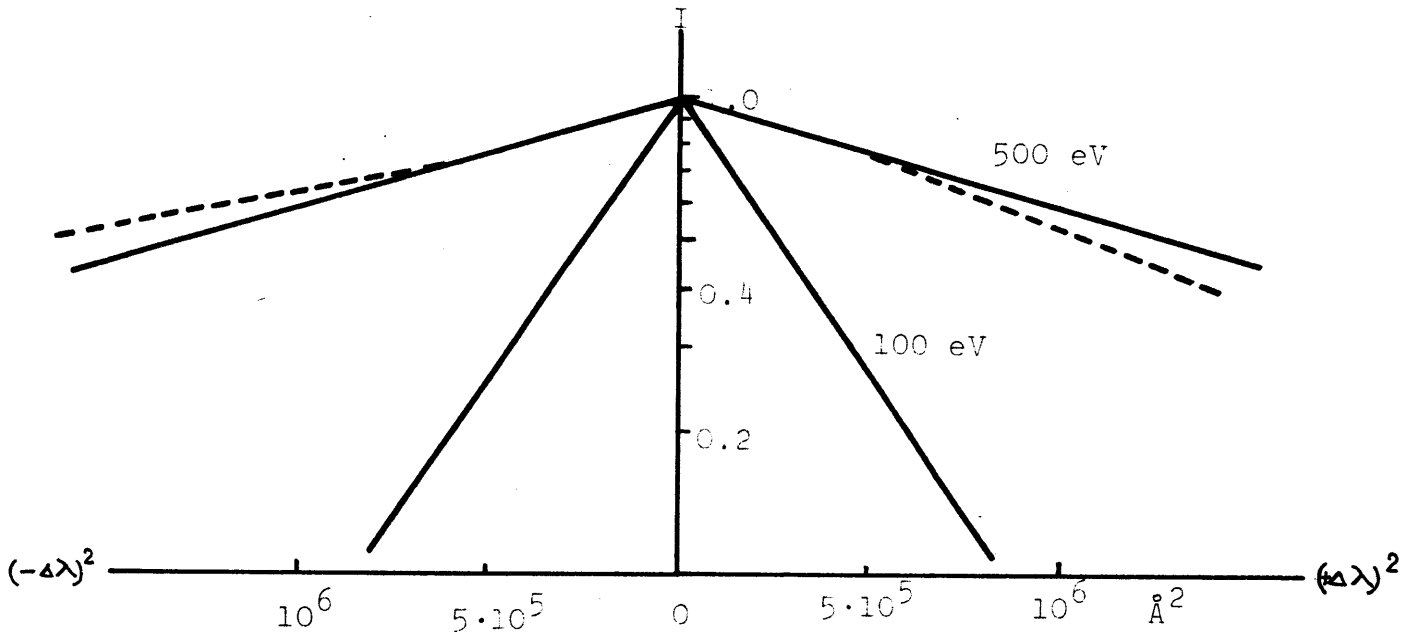

Fig.2 Spectrum of scattered light at right angle for 100 and 500 eV. Dotted curve shows the corrected one for 500 eV.